Silica-based gas separation membranes: Structure–performance relationships across the Si–O continuum from polysilsesquioxanes to amorphous SiO$_2$

Hyo Jung Kim [a,1], Mohamed Gamal Mohamed [b,1], Hyun Jung Yu [c,1], Seo Hyeon Baek [a], Iqubal Hossain [a], Shiao-Wei Kuo [b,*], Jong Suk Lee [a,d,**]

[a] Department of Chemical and Biomolecular Engineering, Sogang University, 35 Baekbeom-ro, Mapo-gu, Seoul, 04107, Republic of Korea
[b] Department of Materials and Optoelectronic Science, Center for Functional Polymers and Supramolecular Materials, National Sun Yat-Sen University, Kaohsiung, 804, Taiwan
[c] Clean Energy Conversion Center, Institute for Advanced Engineering, 175-28, Goan-ro 51 beon-gil, Baegam-myeon, Cheoin-gu, Yongin-si, Gyeongggi-do, 17180, Republic of Korea
[d] Institute of Energy and Environment, Sogang University, 35, Baekbeom-ro, Mapo-gu, Seoul, 04107, Republic of Korea

ARTICLE INFO

ABSTRACT

Membrane technology offers an energy-efficient and compact alternative to conventional thermally driven separation processes. However, polymeric membranes are limited by the permeability–selectivity trade-off, plasticization under high-pressure conditions, and physical aging. To overcome these limitations, two promising classes of silica-based membranes have emerged: (1) amorphous silica membranes fabricated via sol-gel or chemical vapor deposition (CVD), and (2) hybrid and composite membranes incorporating polyhedral oligomeric silsesquioxanes (POSS) or ladder-like polysilsesquioxanes (LPSQ) into polymer matrices. This review provides a comprehensive comparison of these silica-based membrane platforms, with a focus on their structure–performance relationships and application-specific advantages. In polysilsesquioxane (PSQ)-based systems, blending, copolymerization, and crosslinking strategies are shown to improve permeability, interfacial compatibility, and plasticization resistance. In contrast, amorphous silica membranes benefit from rigid Si–O–Si networks that enable molecular sieving, with pore size and connectivity tailored through parameters such as precursor type, pH, dopant addition, and thermal treatment. By consolidating recent progress in both material classes, this review highlights the critical role of molecular-level structural control in achieving targeted gas separation performance and offers a design-oriented perspective on the development of scalable, robust hybrid membranes for industrial separations, including low-pressure CO$_2$ capture and high-temperature H$_2$ purification.

1. Introduction

Membrane technology offers an energy-efficient and compact alternative to conventional thermally driven separation processes such as cryogenic distillation, pressure swing adsorption, and chemical scrubbing [1–4]. However, polymeric membranes face inherent challenges, including the permeability–selectivity trade-off [5], plasticization under high-pressure exposure to condensable gases [6–8], and physical aging arising from polymer chain densification [8,9].

Two complementary strategies have emerged to address these issues:

(1) the development of organic-inorganic hybrid membranes using siloxane-based additives, particularly polysilsesquioxanes (PSQs), and (2) the fabrication of amorphous silica molecular sieve membranes, mainly through sol-gel and chemical vapor deposition (CVD) methods. **PSQs** are organic–inorganic hybrid materials with the general formula [RSiO$_{1.5}$]$_n$, where R denotes an organic group [10–14]. Their structural diversity—including randomly branched (RSQ), cage-like (POSS), and ladder-like (LPSQ) architectures—makes them ideal candidates for tuning membrane properties such as permeability, plasticization resistance, and mechanical strength (Fig. 1) [15–18]. POSS nanoparticles,

due to their nanometer-scale size (1.5–3 nm) and functional tunability (e.g., mono-, di-, and multifunctional forms), have been widely investigated as fillers or crosslinkers in polymer matrices, enabling enhanced free volume and structural rigidity (Fig. 2) [19–22]. LPSQs, in particular, possess a double-stranded siloxane backbone that increases chain rigidity and suppresses aging and plasticization. These PSQs can be incorporated via blending, copolymerization, or cross-linking, often using tailored organic functionalities to ensure compatibility with diverse polymer matrices.

On the other hand, amorphous silica membranes prepared via sol-gel or CVD exhibit intrinsic molecular sieving characteristics [23–28]. These inorganic membranes offer advantages such as high thermal stability, tunable microporosity, and excellent chemical resistance, making them particularly suitable for high-temperature and harsh chemical environments. Fine-tuning their pore size, connectivity, and network structure is achieved through careful control of synthesis conditions—including precursor selection, hydrolysis/condensation ratios, calcination temperature, and doping with metal ions or organic templates [29–33]. These advancements have extended the operating envelope of silica membranes and improved their selectivity for various gas pairs (e.g., H_2/CH_4, CO_2/N_2), although challenges related to hydrothermal stability and scalability remain active areas of research [34–37].

In this review, we aim to provide a comprehensive overview of silica-based membranes for gas separation, covering both (1) PSQ-containing composite membranes, where tailored organic-inorganic interfaces enable improved mechanical and transport properties, and (2) amorphous silica molecular sieve membranes, where the inorganic framework offers inherent size-selective transport under harsh conditions. The review is organized to highlight the structure–performance relationships of PSQs (with emphasis on POSS and LPSQ) and their integration strategies with polymer matrices, as well as recent advances in amorphous silica membrane synthesis, doping, and performance tuning. Particular attention is paid to how the morphology, functionalization, and loading of these materials affect gas transport properties such as permeability, selectivity, and stability. By drawing comparison between these two material classes—PSQs and amorphous silica—we aim to elucidate their respective strengths, limitations, and future directions, ultimately offering design principles for the next generation of high-performance gas separation membranes.

2. Organic-inorganic composite membranes

PSQs can be easily functionalized with a wide range of organic groups, such as amine, phenol, hydroxyl, and others, to enhance their compatibility with polymer matrices [38]. These functional groups enable strong interactions with polymer chains, including hydrogen bonding, and can also facilitate the formation of covalent cross-links, further strengthening the composite structure. Composite membranes incorporating PSQs into polymer matrices can be categorized based on the nature of the interaction between the components. In simple blending, there is no covalent bonding between PSQs and the polymer, relying instead on non-covalent interactions for compatibility. In contrast, copolymerization and cross-linking involve the formation of covalent bonds between PSQs and polymer chains, resulting in a more integrated and stable composite structure. This versatility in tailoring PSQs with functional groups enables the design of advanced composite membranes with enhanced performance for gas separation and other applications.

2.1. Organic-inorganic composite membranes via simple blending

Polymer/PSQ composite membranes are typically fabricated using simple blending, a straightforward and effective method for incorporating additives into polymer matrices. This technique improves the mechanical properties and gas separation performance of the membranes, with interfacial interactions—such as hydrogen bonding, van der Waals and π-π interactions, and other forces—playing a pivotal role in determining their overall efficacy. Glassy polymers with high fractional free volume (FFV) are especially appealing for gas separation applications due to their ability to achieve a favorable balance between permeability and selectivity. Among these, polymers with intrinsic microporosity (PIMs) are particularly noteworthy for their outstanding gas separation performance, which arises from their rigid molecular structure and inherent microporosity [39,40]. Despite these advantages, significant challenges persist, including permeability loss due to the
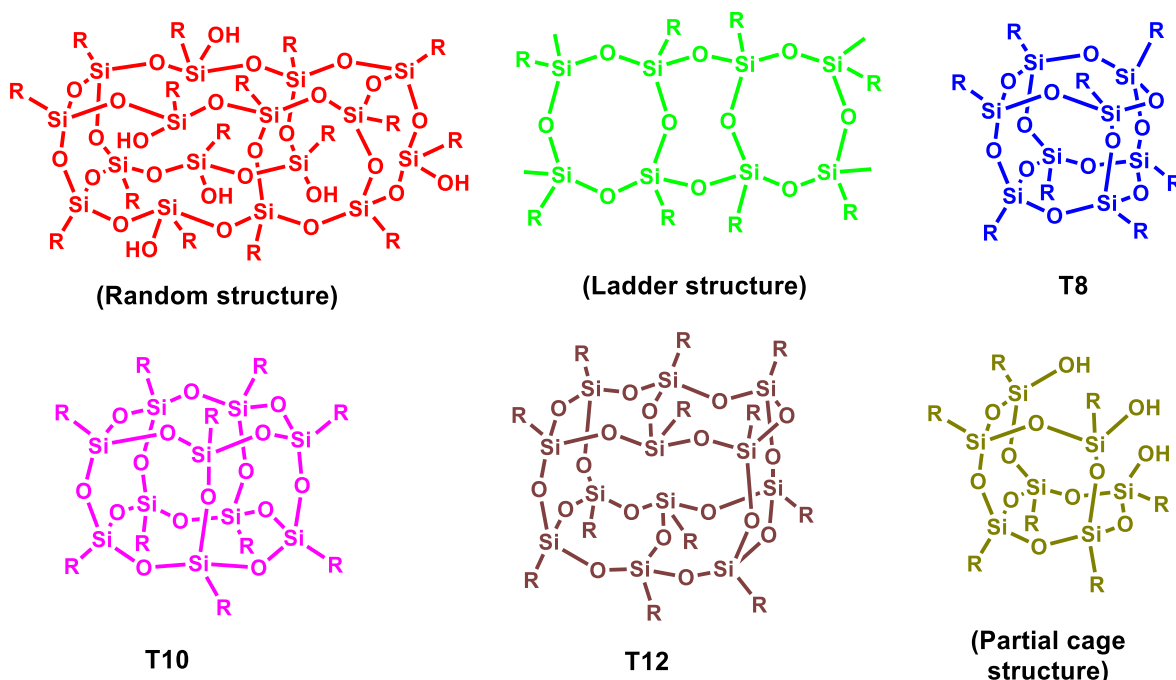

Fig. 1. Types of silsesquioxanes and their structures (Copyright from Ref. [15]).
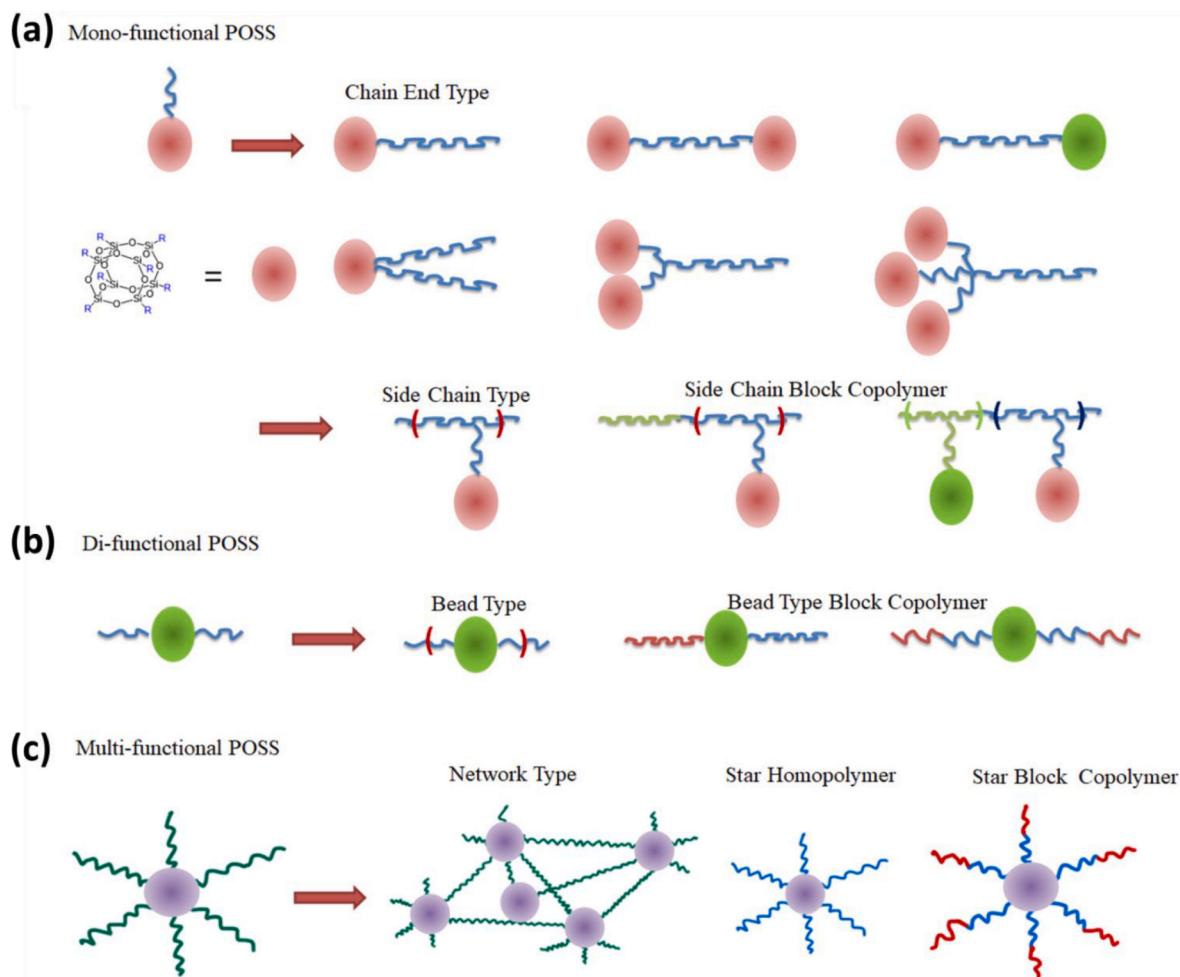
Fig. 2. Organic/inorganic POSS hybrids with diverse architectures formed using (a) mono-functionalized, (b) di-functionalized, and (c) multi-functionalized POSS cages (Copyright from Ref. [22]).

reduction of FFV and selectivity degradation caused by plasticization from condensable gases.

To overcome these challenges, strategies to enhance the interfacial compatibility between PSQs and polymer matrices have been developed. Functionalizing POSS with polar or bulkier substituents has proven effective in improving dispersibility within the polymer matrix and enhancing gas separation performance. Notably, optimizing the interface between POSS and PIM-1 has been identified as a critical factor in achieving superior gas transport properties, paving the way for the development of advanced composite membranes with enhanced stability and efficiency.

Yong et al. demonstrated the advantages of incorporating disilanolisobutyl POSS into polymer of intrinsic microporosity (PIM-1) membranes to mitigate aging and plasticization (Fig. 3a) [41]. PIM-1 possesses a rigid and contorted spirobisindane-based backbone that creates interconnected microporosity, facilitating high gas permeability. At an optimal loading of 2 wt%, the composite membrane exhibited a 40.8 % increase in CO_2 permeability and an 11.4 % improvement in CO_2/CH_4 selectivity compared to pure PIM-1. The improved gas diffusivity was attributed to increased free volume resulting from disrupted polymer chain packing. However, at loadings above 10 wt%, POSS agglomeration caused the space filling and polymer chain rigidification, leading to a significant 67.3 % reduction in CO_2 permeability. Importantly, the inclusion of POSS nanoparticles effectively suppressed CO_2-induced plasticization under mixed CO_2/CH_4 gas conditions at pressures up to CO_2 partial pressure of 15 atm (Fig. 3b and c) and reduced physical aging over 120 days compared to neat PIM-1 (Fig. 3d).

These results highlight the critical need to optimize POSS loading to achieve enhanced permeability and controlled segmental mobility of polymeric chains, thereby ensuring improved membrane performance under high-pressure and long-term operating conditions.

Konnertz et al. investigated the effects of phenethyl-substituted POSS (PhE-POSS) on PIM-1 membranes, focusing on van der Waals and π-π interactions between the phenyl rings of PhE-POSS and the aromatic moieties of PIM-1 (Fig. 4a) [42]. At a loading of 1 wt%, PhE-POSS improved CO_2 permeability while maintaining a consistent CO_2/CH_4 selectivity (Fig. 4b). This enhancement was attributed to a looser, more open polymer structure induced by PhE-POSS incorporation. However, at higher loadings (7.5 wt%), aggregated PhE-POSS particles occupied the polymer's free volume and acted as impermeable barriers, leading to reduced permeability. Notably, the PIM-1-01 membrane (containing 1 wt% PhE-POSS) effectively suppressed CO_2-induced plasticization at pressures up to 20 bar, whereas both neat PIM-1 and the PIM-1-075 membrane exhibited plasticization under the same conditions (Fig. 4c). These findings indicate that even subtle changes in free volume from POSS loading can significantly impact gas transport properties, highlighting the need to optimize POSS content to achieve desirable membrane performance.

Kinoshita et al. explored the impact of functionalizing POSS on its dispersion and interaction within PIM-1 membranes. Functionalized variants, such as octa-nitrophenyl POSS (ONPS) and octa-amino phenyl POSS (OAPS), exhibited significantly better dispersion and interfacial compatibility compared to non-functionalized octa-phenyl POSS (OPS) (Fig. 5a) [43]. Among these, OAPS showed the strongest hydrogen
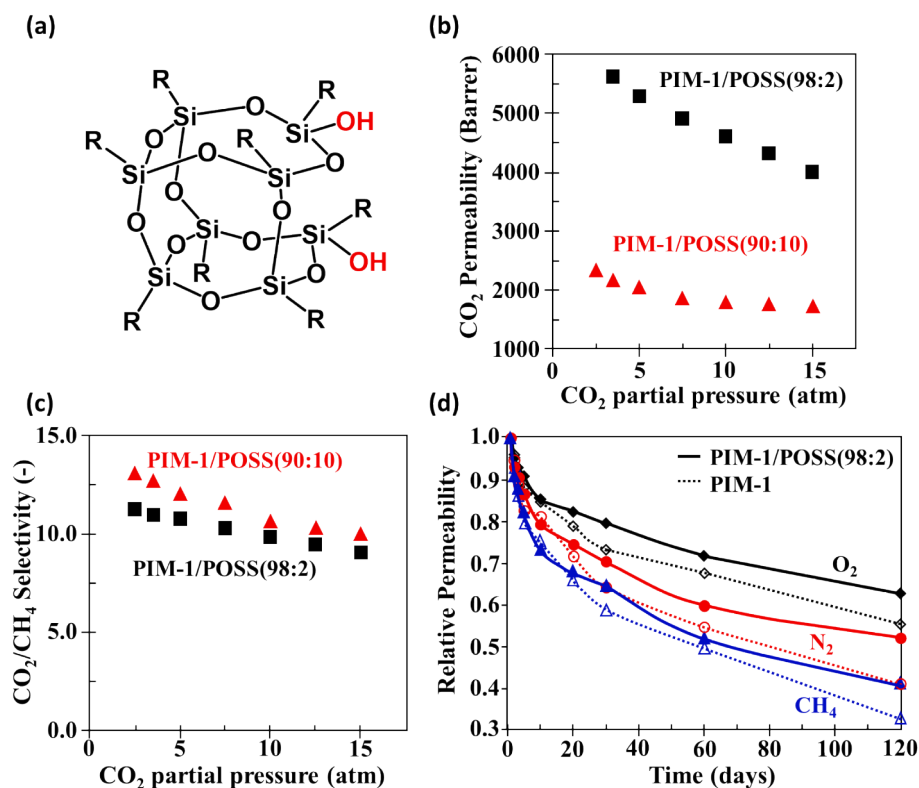
Fig. 3. (a) Chemical structure of disilanolisobutyl-POSS, (b) binary mixed-gas separation performance of PIM-1/POSS (98:2) and PIM-1/POSS (90:10) composite membranes for CO_2 partial pressure, (c) CO_2/CH_4 selectivity, and (d) aging study of PIM-1/POSS (98:2) and PIM-1 membranes (Copyright from Ref. [41]).
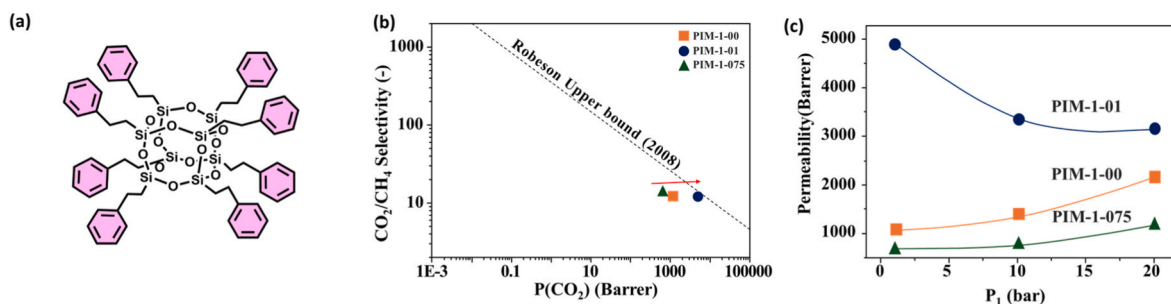

Fig. 4. (a) Chemical structure of phenethyl POSS, (b) CO_2/CH_4 selectivity as a function of CO_2 permeability, with the line representing the 2008 Robeson upper bound. (c) CO_2 permeability as a function of upstream pressure (P_1) (Copyright from Ref. [42]).

bonding with the PIM-1 matrix. At an optimal loading of 5 wt% OAPS, the composite membrane demonstrated substantial selectivity enhancements—30 % for O_2/N_2, 33 % for CO_2/N_2 and CO_2/CH_4, and over 60 % for H_2/N_2 and H_2/CH_4, while maintaining high permeability despite some reduction. This selectivity enhancement was attributed to the increased rigidity of the filler-surrounding polymers, resulting from the nanometric distribution of OAPS and the free volume reduction in the vicinity of the POSS. However, higher loadings beyond 10 wt% resulted in particle aggregation, leading to significant permeability declines. Aging tests revealed that OAPS-functionalized membranes aged 40 % slower under N_2 and 35 % slower under CO_2 compared to neat PIM-1 (Fig. 5b). This improved stability was attributed to the enhanced rigidity of the polymer chains and restricted densification of free volume. These findings highlight the potential of functionalized POSS, particularly OAPS, to enhance both the separation performance and durability of PIM-1-based membranes.

Mohsenpour et al. reported the integration of graphene oxide functionalized with POSS (GO-POSS) into PIM-1 membranes (Fig. 6a) [44].

The functionalization enhanced interfacial compatibility through hydrogen bonding between the amide groups of GO-POSS and the cyano groups of PIM-1 (Fig. 6b). At an optimal loading of 0.05 wt% GO-POSS with prolonged functionalization (72PGP0.05), the composite membrane achieved a remarkable 108 % increase in CO_2 permeability, from 6688 Barrer in neat PIM-1 to 13,944 Barrer, while maintaining a CO_2/CH_4 selectivity of 14.1, compared to 17.0 for neat PIM-1 (Fig. 6c). The result is attributed to the additional free volume and gas diffusion pathways created within the PIM matrix by the incorporation of GO-POSS, leading to enhanced gas permeability. Simultaneously, the increased path tortuosity caused by the horizontally aligned GO laminates can hinder the diffusion of larger molecules while offering near-frictionless channels for smaller ones, thereby enhancing or maintaining selectivity. Furthermore, the incorporation of GO-POSS mitigated the time-dependent decline in permeability, highlighting the role of enhanced interfacial compatibility between fillers and PIM-1 in improving the membrane's anti-aging performance (Fig. 6d).

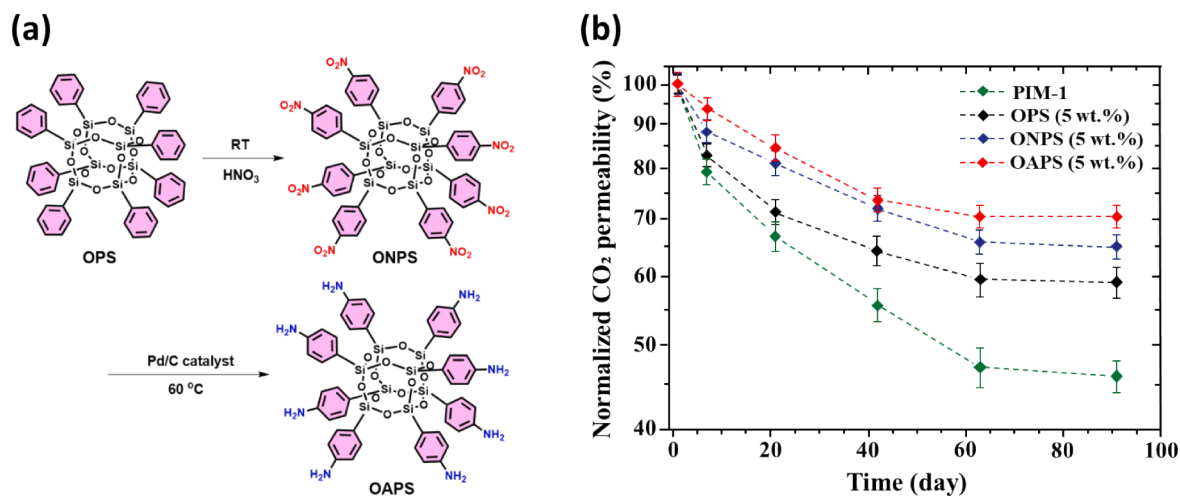Aside from glassy PIM-1, poly(ether-block-amide) (Pebax), a rubbery

Fig. 5. (a) Schematic representation of the reaction steps for the functionalization of POSS (OPS) particles to nitro-POSS (ONPS) and amino-POSS (OAPS) particles, and (b) influence of different POSS particles on long-term CO_2 permeability (Copyright from Ref. [43]).
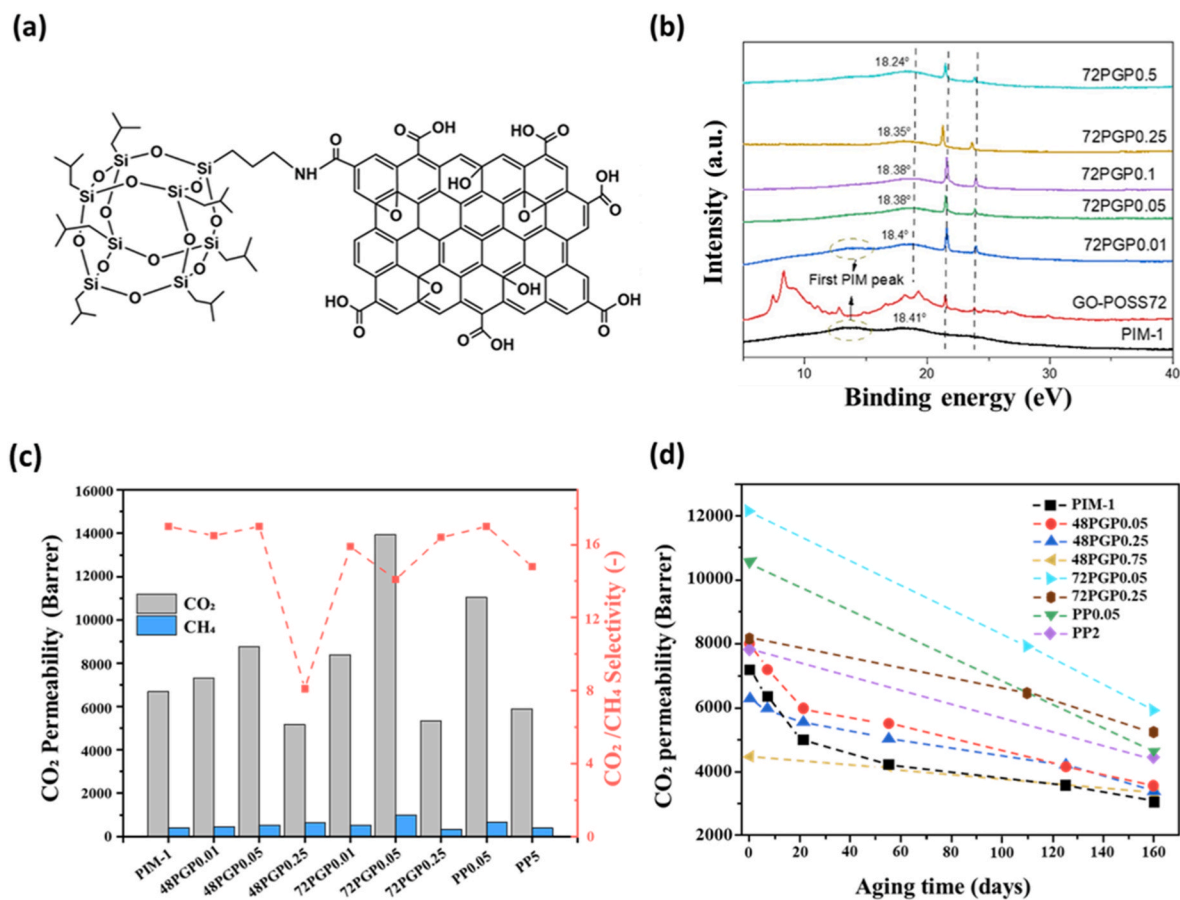

Fig. 6. (a) Chemical structure of graphene oxide functionalized with aminopropyl-isobutyl POSS, (b) XRD patterns, (c) CO_2/CH_4 separation performance, and (d) time-dependent CO_2 permeability of PIM-1 and MMMs (Copyright from Ref. [44]).

block copolymer composed of soft polyether and rigid polyamide segments, has emerged as a promising candidate for CO_2 separation. The crystalline polyamide blocks provide excellent mechanical stability, while the soft polyether blocks—particularly polyethylene oxide (PEO)—exhibit strong CO_2-philic behavior owing to their polar ether groups. Despite its superior processability and inherent affinity and selectivity for CO_2, however, Pebax suffers from relatively low CO_2 permeability [45].

To address this limitation, Polak et al. developed phenyl-functionalized POSS (POSS-Ph) composite membranes based on PEBAX® 2533 (Fig. 7a) [46]. POSS-Ph possesses an $R_8Si_8O_{12}$ cage structure in which all eight Si atoms are substituted with phenyl groups, forming rigid aromatic cages capable of π–π interactions with CO_2 molecules. POSS-Ph was incorporated at concentrations of 0.75, 2, and 8 wt%. The CO_2 permeability of pristine PEBAX® 2533 (210.4 Barrer) increased to 236.1 Barrer and 240.2 Barrer in composite membranes
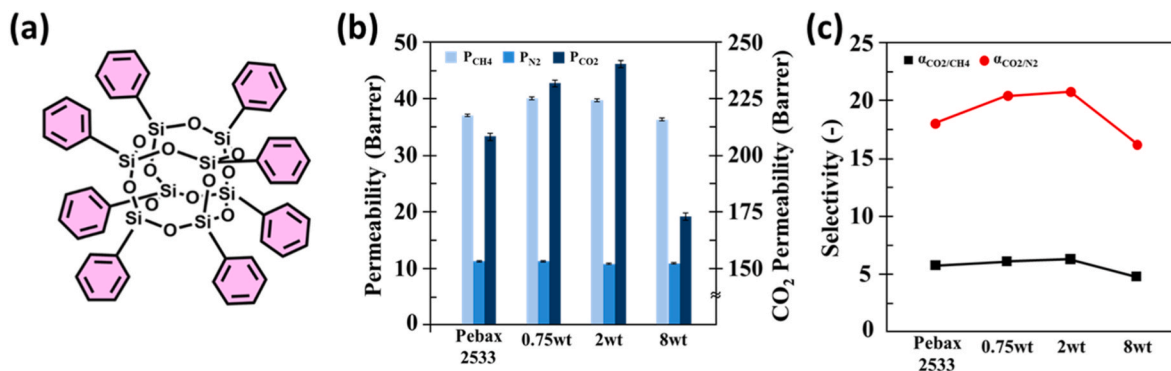
Fig. 7. (a) Chemical structure of phenyl-functionalized POSS, (b) permeability of test gases for membranes with different POSS-Ph concentrations, (c) CO_2/CH_4 and CO_2/N_2 selectivities for membranes with different POSS-Ph concentrations (Copyright from Ref. [46]).

containing 0.75 and 2 wt% POSS-Ph, respectively. Additionally, the ideal selectivities for CO_2/N_2 and CO_2/CH_4 separation improved from 17.98 to 5.66 in pristine PEBAX® 2533 to 21.82 and 6.08 in the 2 wt% POSS-Ph membrane (Fig. 7b and c). The enhancement in CO_2 permeability and CO_2 selectivity (over N_2 and CH_4) was attributed to increased CO_2 solubility upon POSS-Ph incorporation, likely driven by π-π interactions between the phenyl groups of POSS-Ph and CO_2 molecules. However, at higher filler concentrations, membrane performance deteriorated. This decline was attributed to particle aggregation and the rigidification of polymer chains surrounding the filler particles. These findings indicate the existence of a critical filler concentration beyond which gas separation performance diminishes.

Rahman et al. explored the incorporation of POSS into Pebax by introducing PEG-functionalized POSS (PEG-POSS) nanocages into two Pebax grades: PEBAX® MH 1657, which contains polyethylene oxide (PEO) segments with a higher ether oxygen content, and PEBAX® 2533, which contains poly(tetramethylene oxide) (PTMO) segments with a lower ether oxygen content (Fig. 8a–f) [47]. PEG-POSS also features an $R_8Si_8O_{12}$ core, where all Si atoms are functionalized with poly(ethylene glycol) chains, imparting flexible and hydrophilic characteristics that enhance compatibility with PEO-rich matrices while reducing affinity toward PTMO-based ones. The addition of PEG-POSS increased the polyether content in the nanocomposites, as PEG-POSS has a higher polyether weight fraction than the base polymers. At a loading of 30 wt %, the CO_2 permeability increased significantly—by 108 % for PEBAX® MH 1657 and 32 % for PEBAX® 2533 (Fig. 8a and d). In PEBAX® MH
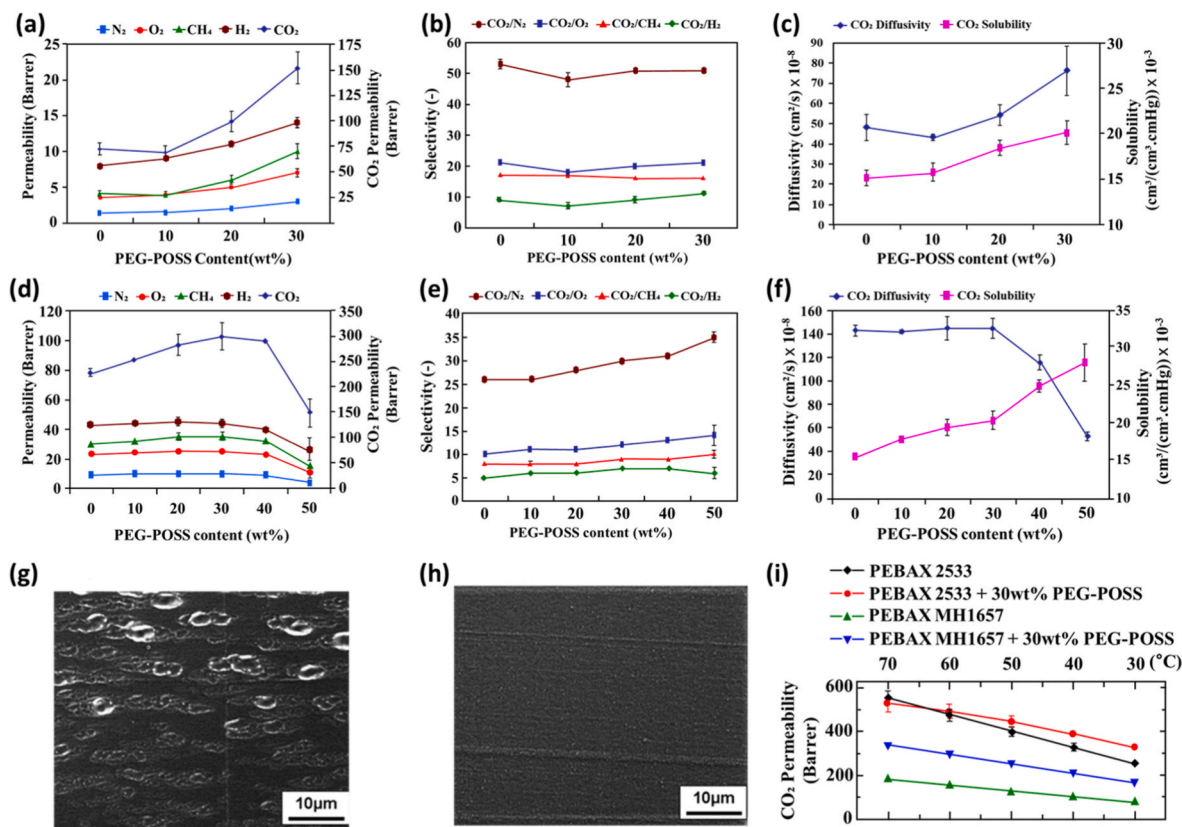

Fig. 8. (a) Single-gas permeability, (b) CO_2 selectivity over light gases, and (c) CO_2 diffusivity and solubility as a function of PEG-POSS content in PEBAX® MH 1657. (d) Single-gas permeability, (e) CO_2 selectivity over light gases, and (f) CO_2 diffusivity and solubility as a function of PEG-POSS content in PEBAX® 2533. Cross-sectional SEM images of (g) PEBAX® 2533 and (h) PEBAX® MH 1657 nanocomposite membranes containing 30 wt% PEG-POSS. (i) Gas permeability as a function of temperature for PEBAX® MH 1657 and PEBAX® 2533 before and after incorporating 30 wt% PEG-POSS (Copyright from Ref. [47]).

1657, both CO_2 diffusivity and solubility increased with PEG-POSS loading up to 30 wt%, while CO_2/CH_4 selectivity remained stable (Fig. 8b and c). Conversely, in PEBAX® 2533, only CO_2 solubility increased, while diffusivity remained nearly unchanged. This resulted in improved CO_2 permeability and CO_2/CH_4 selectivity compared to pristine PEBAX® 2533 (Fig. 8e and f). The enhanced CO_2 solubility in both systems was attributed to the polar oxygen atoms of PEG-POSS, which interact favorably with CO_2 molecules. However, at PEG-POSS loadings above 30 wt% in PEBAX® 2533, CO_2 permeability and diffusivity declined, likely due to agglomeration resulting from limited compatibility between PEG and the structurally dissimilar PTMO segments in PEBAX® 2533 (Fig. 8g). In contrast, better miscibility was observed in PEBAX® MH 1657 due to the structural similarity between the PEG-POSS ligands and the polyether segments (Fig. 8h). Temperature-dependent permeability measurements further confirmed these observations. In PEBAX® MH 1657 containing 30 wt% PEG-POSS, permeability remained consistently higher than that of the neat polymer across the entire temperature range. In contrast, while the permeability of PEBAX® 2533 with 30 wt% PEG-POSS was initially higher, it converged with that of the pristine polymer above 50 °C (Fig. 8i). These results highlight the importance of polymer-filler compatibility, which is strongly influenced by the chemical structure of the base polymer, in optimizing gas separation performance. The findings demonstrate that carefully matching the chemical affinity between PEG-POSS and the matrix polymer is critical to achieving optimal membrane properties.

Building on prior research into POSS-incorporated composite membranes, recent studies have explored the integration of LPSQs—a siloxane-based hybrid component—into a 6FDA-DAM:DABA (3:2) polyimide (PI) matrix for the fabrication of carbon molecular sieve (CMS) membranes, designated as PI-LPSQx [48,49]. The term 6FDA-DAM: DABA refers to a copolyimide synthesized from 4,4′-(hexafluoroisopropylidene)diphthalic anhydride (6FDA) and a diamine mixture of 2,4,6-trimethyl-1,3-diaminobenzene (DAM) and 3,5-diaminobenzoic acid (DABA). CMS membranes, known for their unique pore structures and exceptional separation performance, are considered next-generation membrane technologies [50]. However, a major challenge in the fabrication of polymeric CMS hollow fiber membranes lies in the collapse of their porous substructure during pyrolysis. This collapse is caused by the transition of the polymer from a glassy to a rubbery state prior to decomposition, which severely reduces membrane productivity [51].

To address this issue, the PI-LPSQ precursor was employed to improve the thermal stability of asymmetric hollow fiber membranes during pyrolysis, thereby preserving the porous substructure and enabling the production of high-flux CMS membranes [48]. The incorporation of LPSQ enhanced the rigidity of the PI side chains through hydrogen bonding between the carboxylic acid groups of PI and the pyridyl moieties of LPSQ (Fig. 9a). Additionally, decarboxylation-induced cross-linking at temperatures below the polymer's degradation point provided additional chain rigidification, reinforcing the membrane structure [52]. Solid-state ^{13}C NMR analysis revealed that the addition of LPSQs increased the carbon spin-lattice relaxation time (T_1), particularly in methyl and pendent carboxylic groups (Fig. 9b). This increase in T_1 indicates reduced carbon mobility, confirming that LPSQ effectively rigidifies the polymer side chains. This enhanced rigidity minimized thermal stress-induced substructure collapse during pyrolysis and facilitated the formation of a thin molecular sieve selective layer in the resulting CMS hollow fiber membranes.

Dynamic mechanical analysis (DMA) further supported these findings. As LPSQ content increased, the reduction in storage modulus was mitigated, demonstrating improved resistance to thermal deformation (Fig. 9c). Moreover, the loss modulus peak shifted to higher temperatures, signifying enhanced chain rigidity and superior thermal stress resistance (Fig. 9d). Although the PI-LPSQ20 precursor membrane
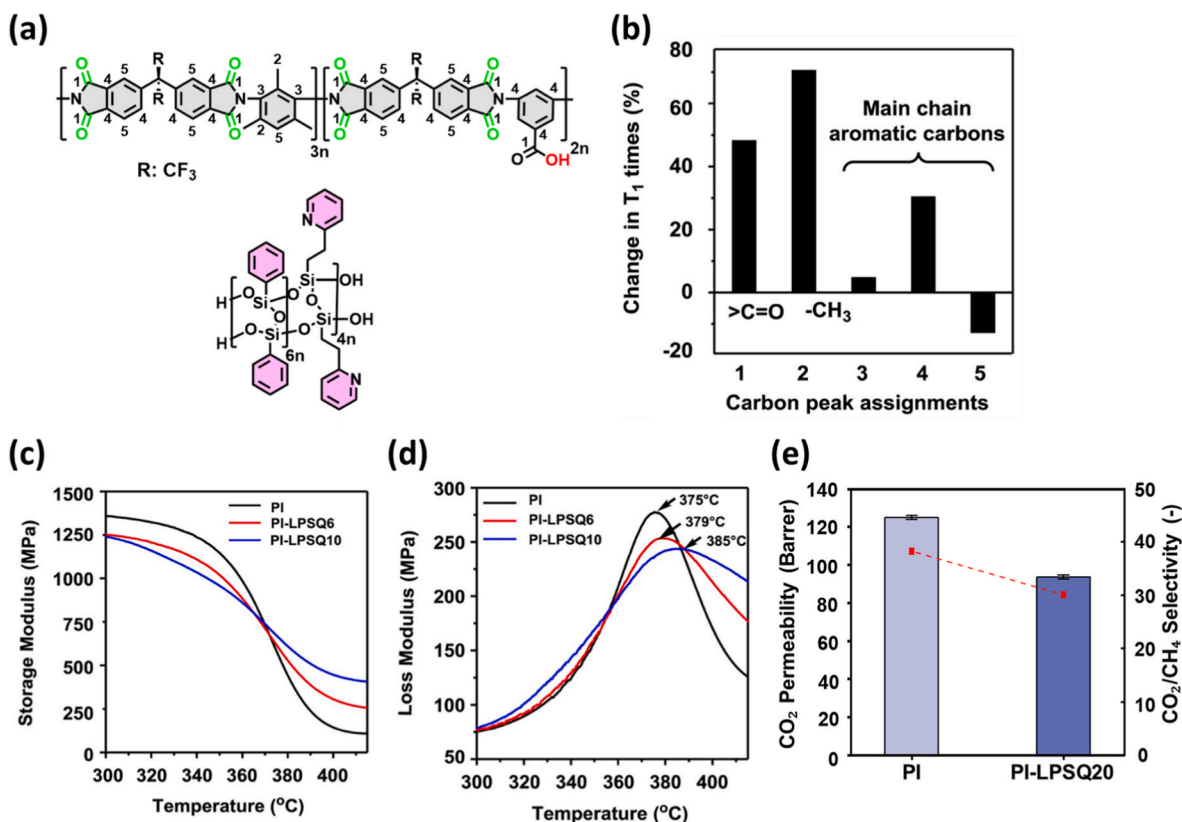

Fig. 9. (a) Carbon peak assignments in PI carbon atoms and the structures of PI and LPSQ, (b) relative change in T_1 of PI carbon atoms for PI-LPSQ20 membranes, with T_1 of carbon atoms in PI membranes set to 0 %, (c) storage modulus and (d) loss modulus of PI, PI-LPSQ6, and PI-LPSQ10 membranes, (e) CO_2/CH_4 separation performance of PI and PI-LPSQ20 (Copyright from Ref. [48]).

exhibited lower CO_2 permeability and CO_2/CH_4 selectivity compared to pristine PI (Fig. 9e), the corresponding CMS PI-LPSQ20 hollow fiber membranes showed remarkable performance improvements. CO_2 permeance and CO_2/CH_4 selectivity increased by 546 % (from 148.0 to 956 GPU) and 50 % (from 33.4 to 50.2) respectively compared to the precursor fibers. These results highlight that LPSQ incorporation plays a critical role in suppressing substructure collapse during pyrolysis. The enhanced chain rigidity provided by LPSQ not only stabilizes the porous architecture but also enables the fabrication of CMS membranes with superior gas separation performance.

2.2. Organic-inorganic composite membranes via copolymerization

Organic-inorganic composite membranes can be effectively prepared through the copolymerization of polymer precursors with POSS macromers. By strategically introducing functional groups at specific sites along the polymer chain—particularly at terminal positions—composite membranes with finely tailored properties can be developed [53–57]. Functional groups such as hydroxyl (-OH), amino (-NH₂), and carboxyl (-COOH) enhance the reactivity, adhesion, and processability of the polymers, enabling stronger interactions with other substances and imparting specialized functionalities to the composite materials. When incorporated as terminal groups, POSS imparts several important advantages, including improved thermal and mechanical stability, oxidation resistance, flame retardancy, and abrasion resistance [58–61]. Additionally, the nanostructure of POSS, especially when functionalized

with organic groups, enhances its solubility in organic solvents and promotes compatibility with polymer matrices through strong physical and chemical interactions.

Dasgupta et al. demonstrated the potential of this approach by preparing a series of polyimide-POSS (PI-POSS) composite membranes. In their study, polyamic acids were end-functionalized with 2 wt% amino-functionalized POSS (NH_2-POSS), as shown in Fig. 10a [62]. Four distinct polyamic acids were synthesized by reacting 2,2-bis(3,4-dicarboxyphenyl) hexafluoropropane (6FDA) with various diamine monomers, including 4,4-bis[3′-trifluoromethyl-4′(4″-aminobenzoxy)benzyl] biphenyl (BAQP), 1,4-bis[3′-trifluoromethyl-4′(4″-aminobenzoxy) benzyl]benzene (BATP), 2,6-bis[3′-trifluoromethyl-4′(4″-aminobenzoxy) benzyl]pyridine (BAPy), and 2,5-bis[3′-trifluoromethyl-4′(4″-aminobenzoxy) benzyl]thiophene (BATh). The resulting 6FDA-BATh-POSS membrane was characterized using field-emission scanning electron microscopy (FESEM), which confirmed the homogeneous distribution of POSS nanocages within the polyimide (PI) matrix (Fig. 10b and c). X-ray diffraction (XRD) and DSC analyses confirmed the amorphous nature of all PI-POSS membranes. Mechanical tests showed that the tensile strength and Young's modulus of the PI-POSS membranes were comparable to those of pristine PI, although their elongation at break was slightly reduced. Notably, the incorporation of POSS nanocages increased the FFV, which enhanced gas permeability, while maintaining CO_2/CH_4 and O_2/N_2 selectivities (Fig. 10d and e). These findings highlight the effectiveness of POSS-based copolymerization strategies in improving gas transport properties without compromising selectivity,
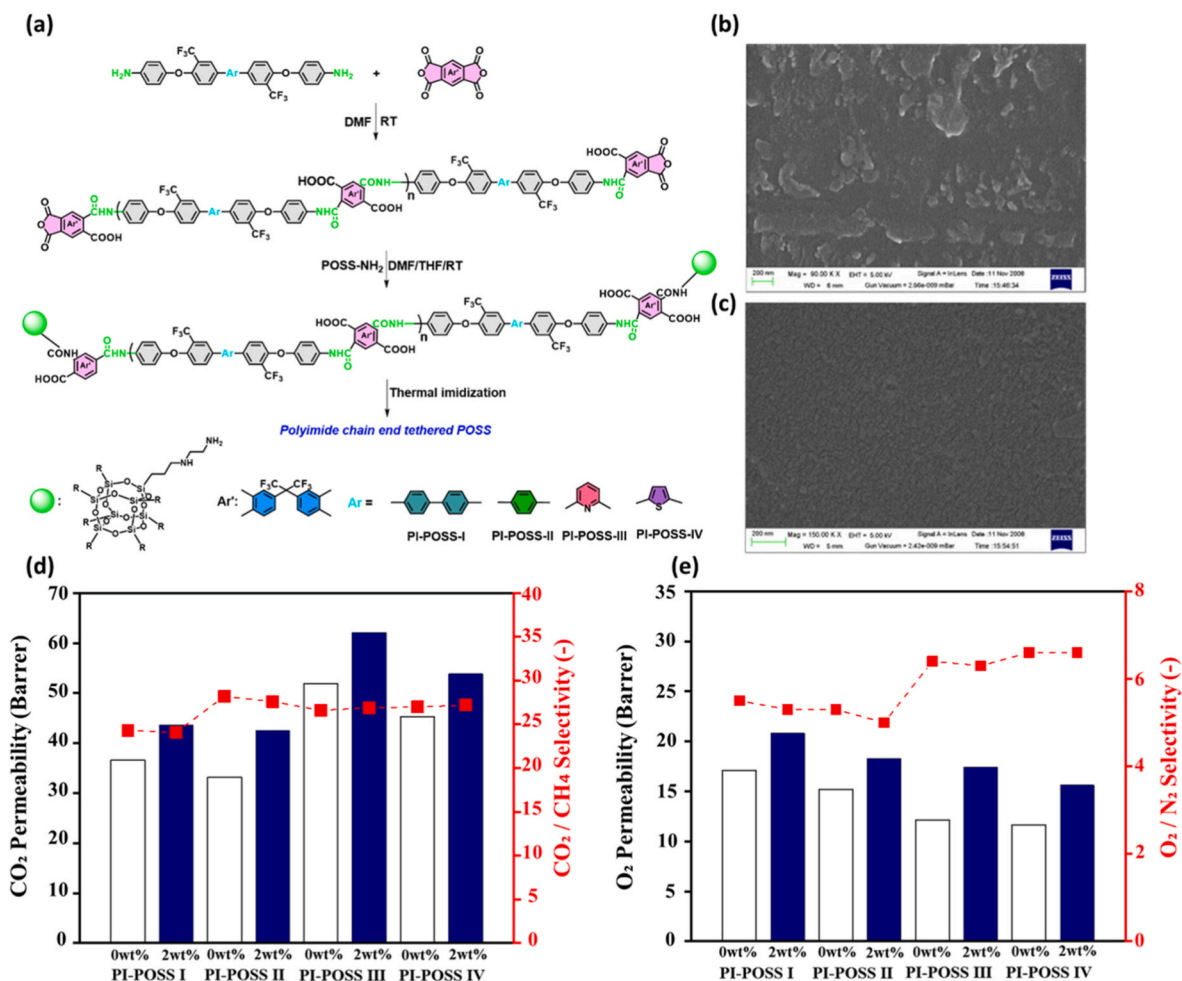

Fig. 10. (a) Reaction scheme and molecular structure of the PI-POSS nanocomposite membranes. FESEM images of (b) a PI-POSS nanocomposite membrane and (c) a pristine PI membrane. Gas permselectivities (α_p) of the PI-POSS nanocomposite membranes: single-gas (d) CO_2/CH_4 and (e) O_2/N_2 separation properties. The gas transport properties of these PI-POSS membranes were measured at 3.5 atm of applied gas pressure at 35 °C (Copyright from Ref. [62]).

and they encourage further exploration of functionalization strategies for advanced membrane design.

Rios-Dominguez et al. further investigated the role of POSS in copolymerized systems by examining the effect of high silica and oxygen atom concentrations in POSS particles on gas transport properties of polystyrene membranes. Polystyrene membranes were synthesized with varying amounts of a POSS-TEMPO macroinitiator to evaluate its influence on membrane performance (Fig. 11a) [63]. In this system, the POSS terminal group was functionalized with hydroxy-TEMPO, a stable free radical, and integrated into a hybrid polystyrene-based polymer (ST1515) through stable free radical polymerization using benzoyl peroxide (BPO) and hydroxy-TEMPO (Fig. 11b). This functionalization facilitated uniform dispersion of POSS cages within the membrane matrix, which increased the FFV and enhanced gas permeability. Membranes containing 5 and 10 wt% POSS-TEMPO achieved an optimal balance between enhanced permeability and preserved selectivity, with performance approaching the Robeson upper bound for gas separation (Fig. 11c). However, at higher POSS-TEMPO loadings (20 wt%), although permeability increased significantly, selectivity declined. This reduction in selectivity, particularly in the PSPOSS20 sample, was attributed to marked increase in N_2 permeability compared to that of O_2, resulting from the enhanced FFV induced by POSS incorporation. DSC analysis showed that the glass transition temperature (T_g) of the membranes increased with POSS loading (Fig. 11d), reflecting the dual role of nanoparticles in polymer dynamics. At lower loadings, nanoparticles like POSS increased chain flexibility and porosity, enhancing gas transport. In contrast, at higher loadings, they restricted segmental mobility, which negatively affected selective gas transport.

2.3. Organic-inorganic composite membranes via cross-linking

Composite membranes can be fabricated through cross-linking, which involves forming a network structure via covalent bonds between polymer chains and additives. This approach effectively enhances
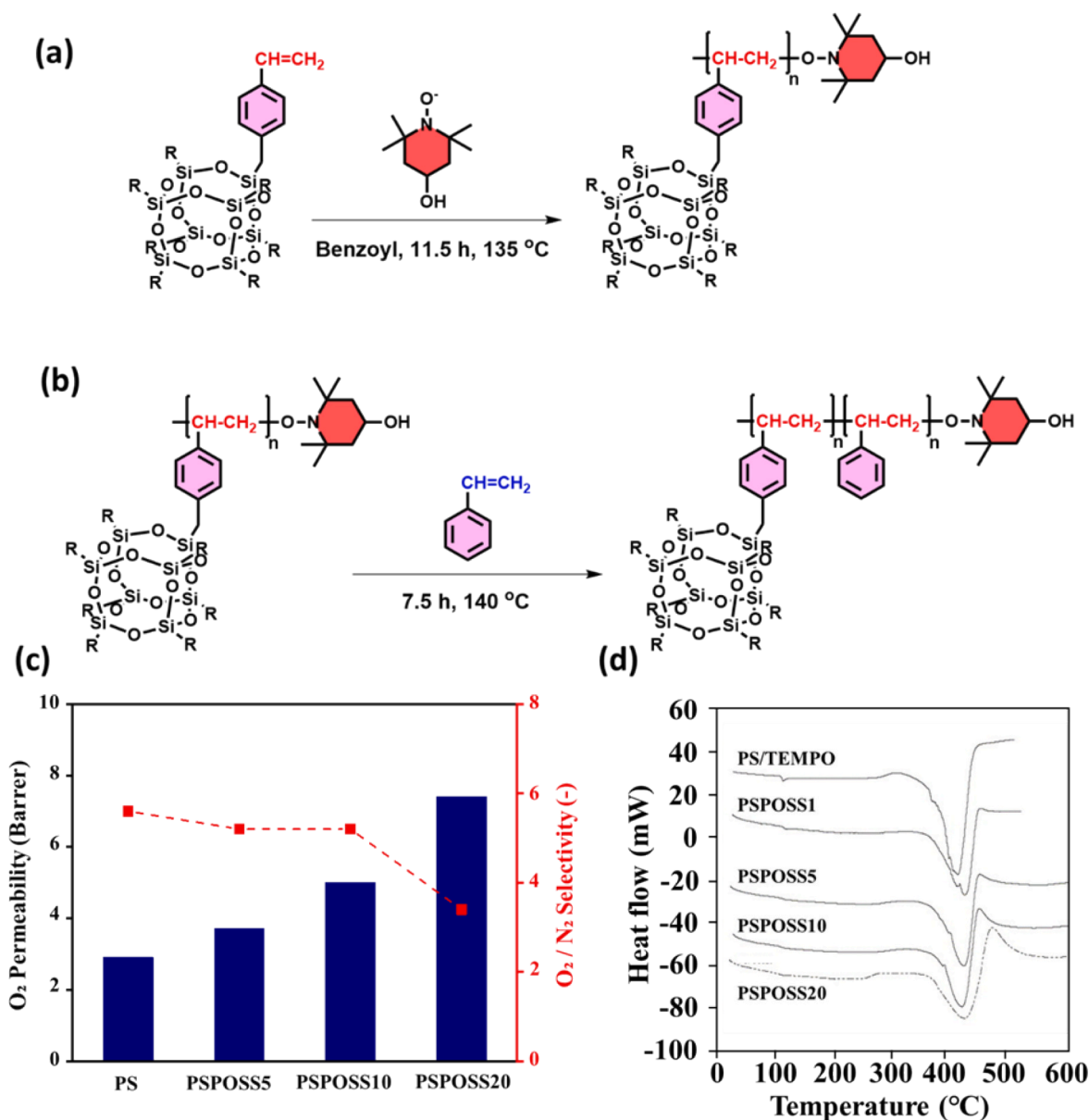

Fig. 11. Solution polymerization reaction pathways for a POSS–TEMPO macroinitiator and polystyrenes synthesized with different macroinitiator loadings where R = *i*-butyl: (a) POSS–TEMPO macroinitiator reaction and (b) PS/POSS–TEMPO polymerization reaction, (c) O_2/N_2 separation performance of polystyrene membranes synthesized with different loads of a POSS–TEMPO macroinitiator, (d) DSC scans for PSPOSS membranes (Copyright from Ref. [63]).

the mechanical properties and plasticization resistance of glassy polymeric membranes, particularly under high feed pressures with condensable gases [64].

The Chung group developed CO_2-selective composite membranes by cross-linking diamine-functionalized polyetheramine (PEA) with glycidyl-POSS (Fig. 12a) [65]. Epoxy-POSS was incorporated into the PEA membranes to inhibit crystallization and improve gas permeability while preserving selectivity. The cross-linked network was formed through a ring-opening reaction between the epoxy groups of glycidyl-POSS and the amino groups of PEA, resulting in a robust structure that enhanced compatibility between the polar ether groups of PEA and the nonpolar POSS domains. Successful cross-linking was confirmed by FT-IR analysis, showing characteristic O–H and N–H stretching bands at 3300-3600 cm^{-1} and N–H scissoring at 1630 cm^{-1}. XRD results further demonstrated that crystallization was effectively suppressed, leading to an amorphous structure conducive to gas transport (Fig. 12b and c). At optimal POSS loading, CO_2 diffusivity significantly improved [66,67]. However, excessive POSS content reduced chain mobility and FFV, limiting further enhancement. Among the PEA-POSS membranes, the sample containing 70 wt% POSS exhibited the highest CO_2 permeability (401 Barrer) while maintaining excellent selectivity, achieving a CO_2/N_2 selectivity of 42.4 and a CO_2/H_2 selectivity of 7.7 at 35 °C and 1 bar (Table 1). Thermal stability was significantly enhanced, as evidenced by increased degradation temperatures in TGA analysis (Fig. 12d), and mechanical strength improvements were confirmed through nanoindentation testing. Long-term stability tests also demonstrated that the PEA 50:50 membrane maintained consistent CO_2 permeability over four days, highlighting the durability of the cross-linked network. Thus, the incorporation of POSS into PEA membranes effectively addresses the limitations of conventional PEA membranes—such as crystallinity and weak intermolecular interactions—offering valuable insights for developing high-performance, durable gas separation membranes.

Li et al. further developed POSS-based composite membranes for CO_2/CH_4 separation by blending chlorinated alkane-polybenzimidazole (CPBI) with amino-functionalized POSS (NH_2-POSS) (Fig. 13a) [68]. The band near 1650 cm^{-1} corresponds to the C=N stretching vibration of the benzimidazole ring. A slight shift in its position and intensity upon NH_2-POSS incorporation suggests a weakening of intermolecular hydrogen bonding due to grafting between the amino groups of NH_2-POSS and the chlorinated CPBI backbone (Fig. 13b). The incorporation of NH_2-POSS disrupted the internal hydrogen bonding of the CPBI chains, increasing d-spacing and promoting gas transport. The CO_2/CH_4 separation performance of CPBI/NH_2-POSS mixed-matrix membranes (MMMs) improved steadily with increasing NH_2-POSS concentrations, reaching optimal performance at 6 wt%. At this concentration, the membrane exhibited a CO_2 permeability of 9 Barrer and a CO_2/CH_4 separation factor of 78 (Fig. 13c). This enhancement was attributed to the creation of low-resistance diffusion pathways for CO_2, facilitated by both specific interactions between the amino groups of NH_2-POSS and CO_2 and the increased molecular spacing in CPBI. However, at higher NH_2-POSS concentrations (e.g., 9 and 12 wt%), agglomeration of nanocages within the CPBI matrix occurred, negatively affecting separation performance. While the mechanical properties (tensile strength, elongation, and Young's modulus) of CPBI/NH_2-POSS MMMs slightly declined with increasing NH_2-POSS content, due to disrupted CPBI chain packing, they remained sufficient for gas separation applications (Fig. 13d).

Building on previous studies, further research explored the incorporation of LPSQs into composite membranes. Yu et al. proposed a novel method to simultaneously enhance gas permeability and plasticization resistance through thermal cross-linking between glassy polyimides
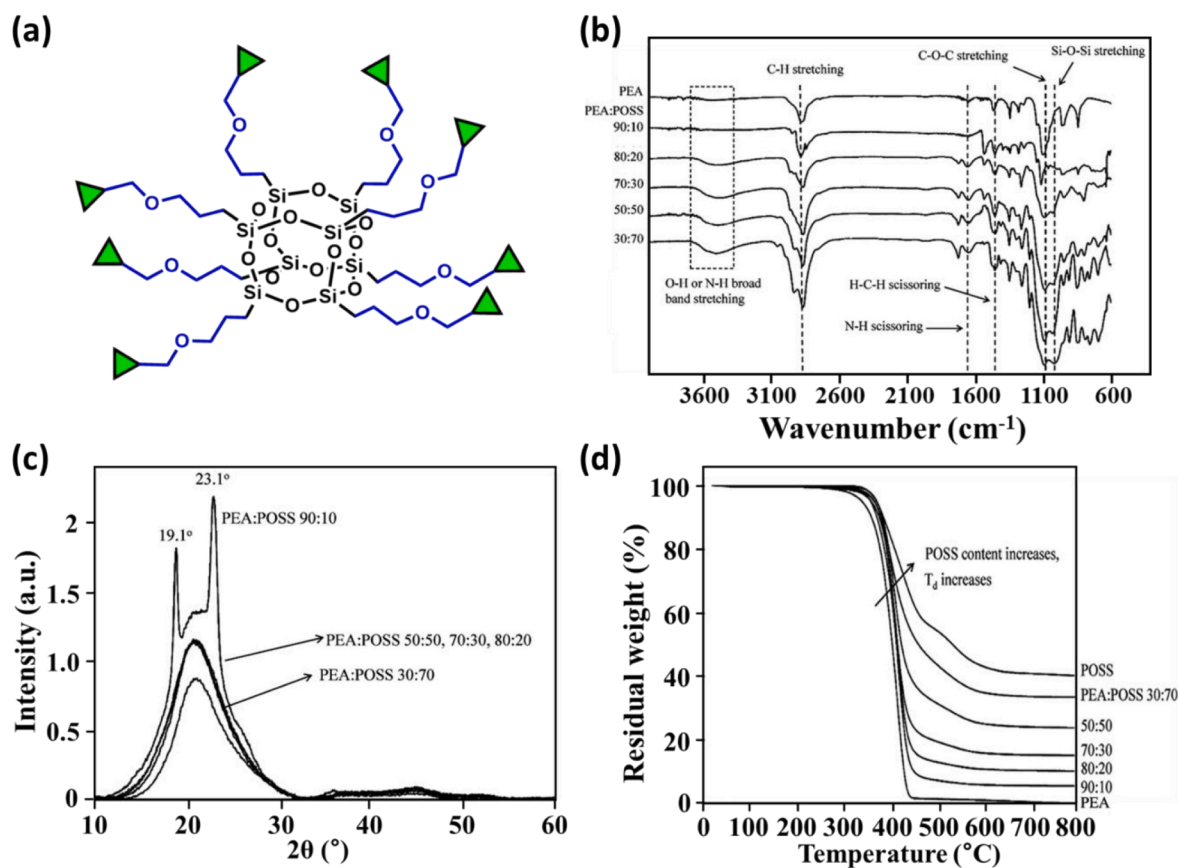

Fig. 12. (a) Chemical structures of glycidyl-POSS, (b) FT-IR spectra, (c) XRD patterns of the hybrid membranes, and (d) TGA curves of the PEA/glycidyl-POSS hybrid membranes (Copyright from Ref. [65]).

(PIs) and LPSQs (Fig. 14a) [69]. The PI matrix corresponds to a series of copolyimides synthesized from 3,3′,4,4′-benzophenonetetracarboxylic dianhydride (BTDA) and a diamine mixture of 2,3,5,6-tetramethyl-1, 4-phenylenediamine (Durene) and 3,5-diaminobenzoic acid (DABA).
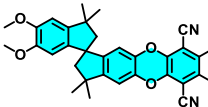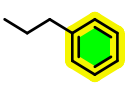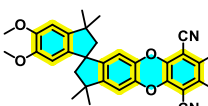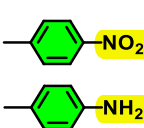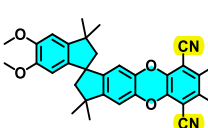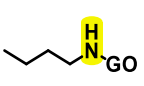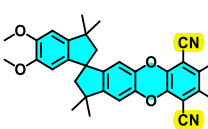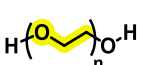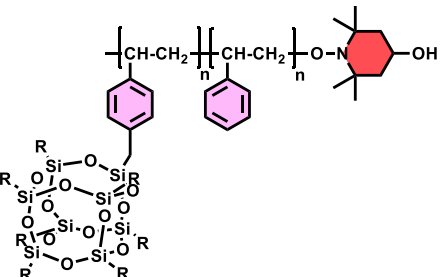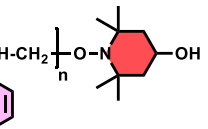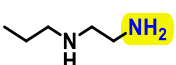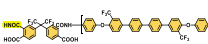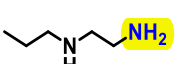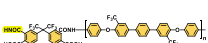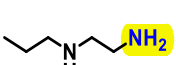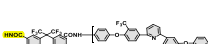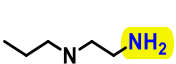
PI-2:1, PI-3:2, and PI-4:1 denote copolyimides prepared with Durene: DABA molar ratios of 2:1, 3:2, and 4:1, respectively. Cross-linking

proceeded via two mechanisms: amidation between the amine groups of LPSQ and the carboxylic acid groups of PI, and decarboxylation of PI side chains. To comparatively assess cage-like versus ladder-like architectures, octa(aminophenyl)silsesquioxane (OAPS), a type of POSS, was also incorporated alongside LPSQ for detailed evaluation.

Nanoindentation tests showed that the incorporation of 20 wt%

Table 1

Polymer matrices and POSS functional groups used in composite membranes via simple blending, copolymerization, and cross-linking, along with their corresponding changes in permeability and selectivity.

No.	Functional group*	Polymer matrix	Loaded weight (%)	ΔP_{CO2} (%)	ΔP_{CH4} (%)	ΔP_{N2} (%)	$\Delta\alpha_{CO2/CH4}$ (%)	$\Delta\alpha_{CO2/N2}$ (%)	Ref
1			2	40.8	35.4	-	11.4	-	41
2			1	347	-	-	≈ 0	-	42
3			5	−20.1	−40.0	−38.7	33.2	30.3	43
4			0.05	109	151	-	−17.1	-	44
5			2	14.2	6.2	−6	7.5	21.3	46
6			30	108	-	-	-	-	47
7			30	32	-	-	-	-	
a			10	-		85.7	-	-	62
b			2	19.1	20.1	26.4	−0.8	−3.6	63
c			2	28.3	31.1	27.2	−2.1	−5.7	
d			2	19.7	18.3	45	1.1	−1.6	
e			2	18.9	18	33.1	0.7	0	

Table 1 (*continued*)

No.	Functional group*	Polymer matrix	Loaded weight (%)	ΔP_{CO2} (%)	ΔP_{CH4} (%)	ΔP_{N2} (%)	$\Delta\alpha_{CO2/CH4}$ (%)	$\Delta\alpha_{CO2/N2}$ (%)	Ref
8			20	−28.7	−11.8	−27.8	−21.1	−4.2	48
A			50	15.5	-	19.8	-	−3.6	65
B			6	197	−14.7	-	248	-	68
C			20	808	711	776	12	3.7	69

LPSQ or OAPS into the PI membrane (e.g. PI-2:1–20 % and PI/OAPS-20 %) significantly reduced both hardness (resistance to plastic deformation) and reduced modulus (resistance to elastic deformation) due to the presence of low-molecular-weight components (Fig. 14b). However, after thermal cross-linking, the PI-2:1–20 % membrane exhibited an increase in hardness and reduced modulus, while cross-linked pristine PI and PI/OAPS-20 % membranes showed further decreases. This distinctive behavior is attributed to the high cross-linking density and rigid, pseudo-2D ladder-like structure of LPSQ, which formed a robust, high-density PI/LPSQ network. Although decarboxylation- and amidation-induced cross-linking led to the formation of larger microvoids in the PI/LPSQ membrane [70], resulting in a slight reduction in modulus, the cross-linked PI/LPSQ membrane remained mechanically tougher than its non-cross-linked counterpart. The rigid ladder-like structure of LPSQ contributed significantly to enhancing mechanical integrity [71,72].

Incorporation of LPSQ into PI membranes initially reduced gas permeability compared to pristine PI, due to the impermeable LPSQ backbone and strong interactions between the carboxylic acid groups of PI and the amine moieties of LPSQ. However, following thermal cross-linking, the permeability of PI/LPSQ membranes improved significantly without a notable loss in selectivity (Fig. 14c). Molecular dynamics (MD) simulations revealed that the accessible volume for penetrants per unit surface area (AV/SA) increased for both PI and PI/LPSQ membranes after cross-linking. This effect was particularly pronounced in PI/LPSQ membranes, where LPSQ promoted the formation of larger and more interconnected cavities within the polymer matrix, leading to a substantial enhancement in CO_2 permeability (Fig. 14d and e). Among the PI/LPSQ membranes, the PI-4:1–20 % composition,

which contained the lowest percentage of carboxylic acid groups, exhibited the highest degree of amidation. This promoted greater cavity connectivity, contributing to higher FFV and gas permeability. In contrast, membranes with higher carboxyl content exhibited reduced permeability due to stronger intermolecular interactions that restricted free volume. Notably, the PI-4:1–20 % membrane achieved the best balance between permeability and selectivity among the tested compositions. In addition to improved permeability, the cross-linked PI/LPSQ membranes demonstrated excellent plasticization resistance. The membranes maintained stable gas separation performance under both single-gas conditions up to 22 bar and CO_2/CH_4 mixed-gas conditions with CO_2 partial pressures up to 12 bar (Fig. 14f). These results clearly demonstrate that the incorporation of LPSQ as a filler significantly enhances both anti-plasticization and gas transport properties in composite membranes.

3. Amorphous SiO_2 molecular sieve membranes

Silica, a prototypical glass-forming oxide, readily forms an amorphous network without requiring additional stabilizing oxides—unlike intermediate oxides such as Al_2O_3, TiO_2, or ZrO_2. Its atomic structure comprises covalently bonded SiO_4 tetrahedra connected in a continuous, three-dimensional network that lacks long-range order. Amorphous silica membranes are typically fabricated on porous substrates via sol-gel processing or CVD, resulting in asymmetric architectures with a thin, selective silica layer. These membranes are especially suited for molecular-scale gas separations due to their facile fabrication, tunable microstructures, favorable gas transport characteristics, and thermal
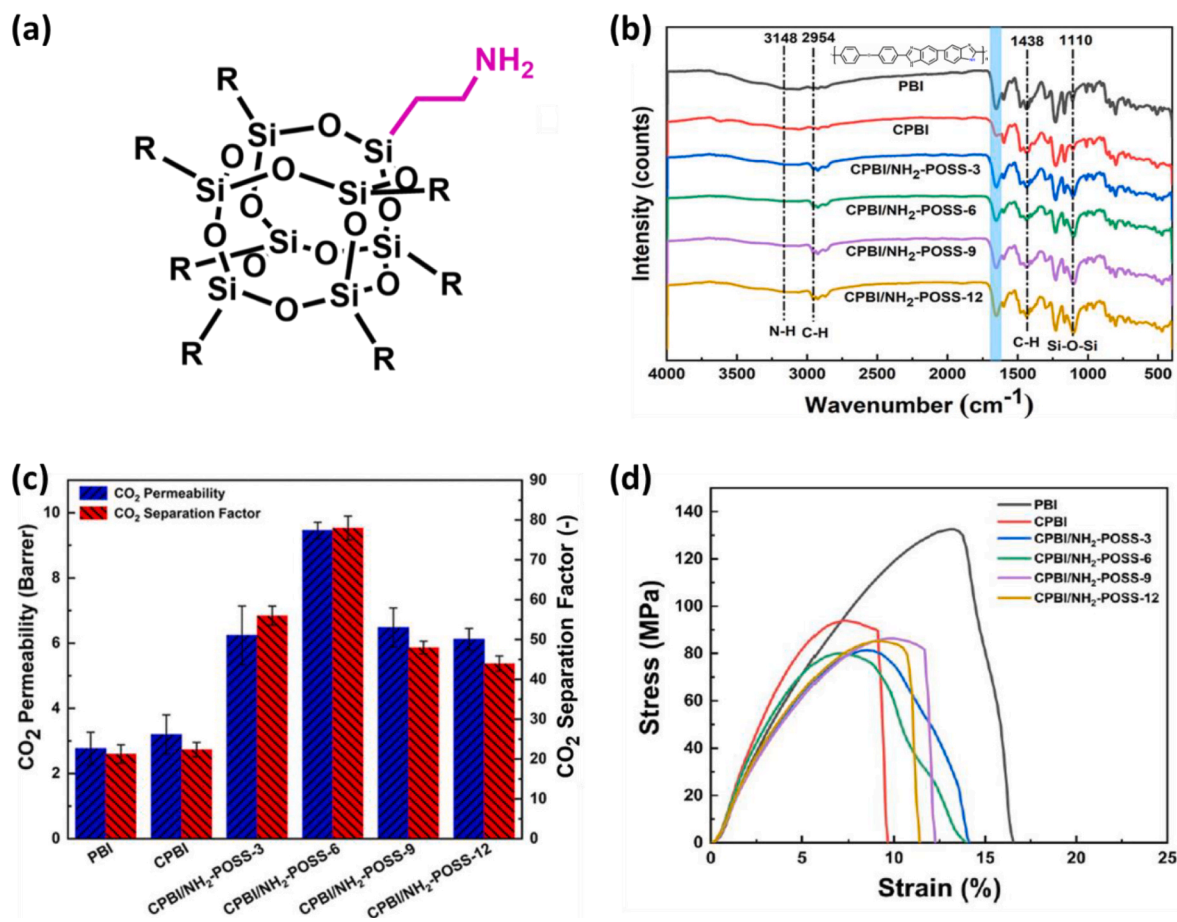
Fig. 13. (a) Chemical structure of NH₂-POSS, (b) FT-IR spectra of PBI, CPBI, and CPBI/NH₂-POSS MMMs (inset: chemical structure of PBI), (c) CO₂/CH₄ separation performance, and (d) stress-strain curves of the membranes. CPBI is a chlorinated derivative of PBI. CPBI/NH2-POSS-x represents denotes composite membranes containing x wt% NH2-POSS (Copyright from Ref. [68]).
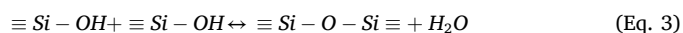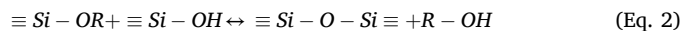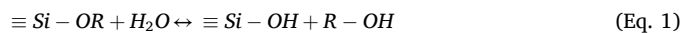
and chemical stability.

3.1. Sol-gel-derived silica membranes

The sol-gel technique is among the most widely studied methods for fabricating amorphous silica membranes. It involves hydrolyzing alkoxysilane precursors such as tetramethoxysilane (TMOS) or tetraethoxysilane (TEOS) to form a colloidal solution (sol), which subsequently undergoes gelation. For asymmetric membrane fabrication, the silica sol is deposited onto a porous support using techniques such as dip-coating, spin-coating, spray coating, or flow-induced coating, resulting in a thin xerogel layer. The coated substrates are then calcined at 300–700 °C to remove residual organics and densify the silica network, thereby improving structural integrity and gas separation performance (Fig. 15) [73]. The thickness of the resulting selective layers typically ranges from 30 to 100 nm, though precise measurement is often challenging due to infiltration into the porous support via capillary action [74–76].

Sol-gel processes can be broadly categorized into two routes based on the structural characteristics of the sol: the colloidal route and the polymeric route. The colloidal route employs a dispersion of pre-formed oxide nanoparticles, while the polymeric route relies on the hydrolysis and polycondensation of alkoxysilanes in alcoholic solvents to form a polymeric silica network. The polymeric route is commonly used to synthesize microporous membranes with pore size below 2 nm, whereas the colloidal route is suited for producing mesoporous layers with pore size between 2 and 50 nm. In the colloidal route, the final pore structure is strongly influenced by the size, shape, and packing of the constituent nanoparticles [77]. For instance, in a system of uniform spherical particles with radius R, a close-packed structure can produce two characteristic pore sizes: approximately $0.225R$ and $0.414R$. In more disordered arrangements, such as random packing, the pore size distribution typically spans from $0.2R$ to $0.6R$ [77]. This structural tunability makes the sol-gel method a versatile approach for tailoring pore architecture to meet specific gas separation requirements. The sol-gel method allows for flexible pore structure tuning, with micropore sizes generally ranging from 0.25 to 0.6 nm depending on precursor chemistry, catalyst conditions, and calcination protocols [78,79].

The overall conversion of alkoxysilanes into silica involves two key steps: hydrolysis and condensation. In the first step, hydrolysis of the alkoxy group yields silanol groups (Eq. (1)). These silanols then participate in condensation reactions either with unreacted alkoxy precursors (Eq. (2)) or with other silanols (Eq. (3)), resulting in the formation of siloxane ($\equiv Si-O-Si\equiv$) bridges that constitute the silica network:

$$\equiv Si-OR + H_2O \leftrightarrow \ \equiv Si-OH + R-OH \qquad (Eq.\ 1)$$

$$\equiv Si-OR + \ \equiv Si-OH \leftrightarrow \ \equiv Si-O-Si \equiv +R-OH \qquad (Eq.\ 2)$$

$$\equiv Si-OH + \ \equiv Si-OH \leftrightarrow \ \equiv Si-O-Si \equiv + H_2O \qquad (Eq.\ 3)$$

These reactions are typically catalyzed by either acidic or basic media, which play a critical role in determining the resulting pore structure. Acidic conditions favor hydrolysis over condensation, leading to extended linear or branched silica chains that are suitable for forming microporous membranes. In contrast, basic conditions accelerate condensation, producing highly cross-linked, aggregated networks that
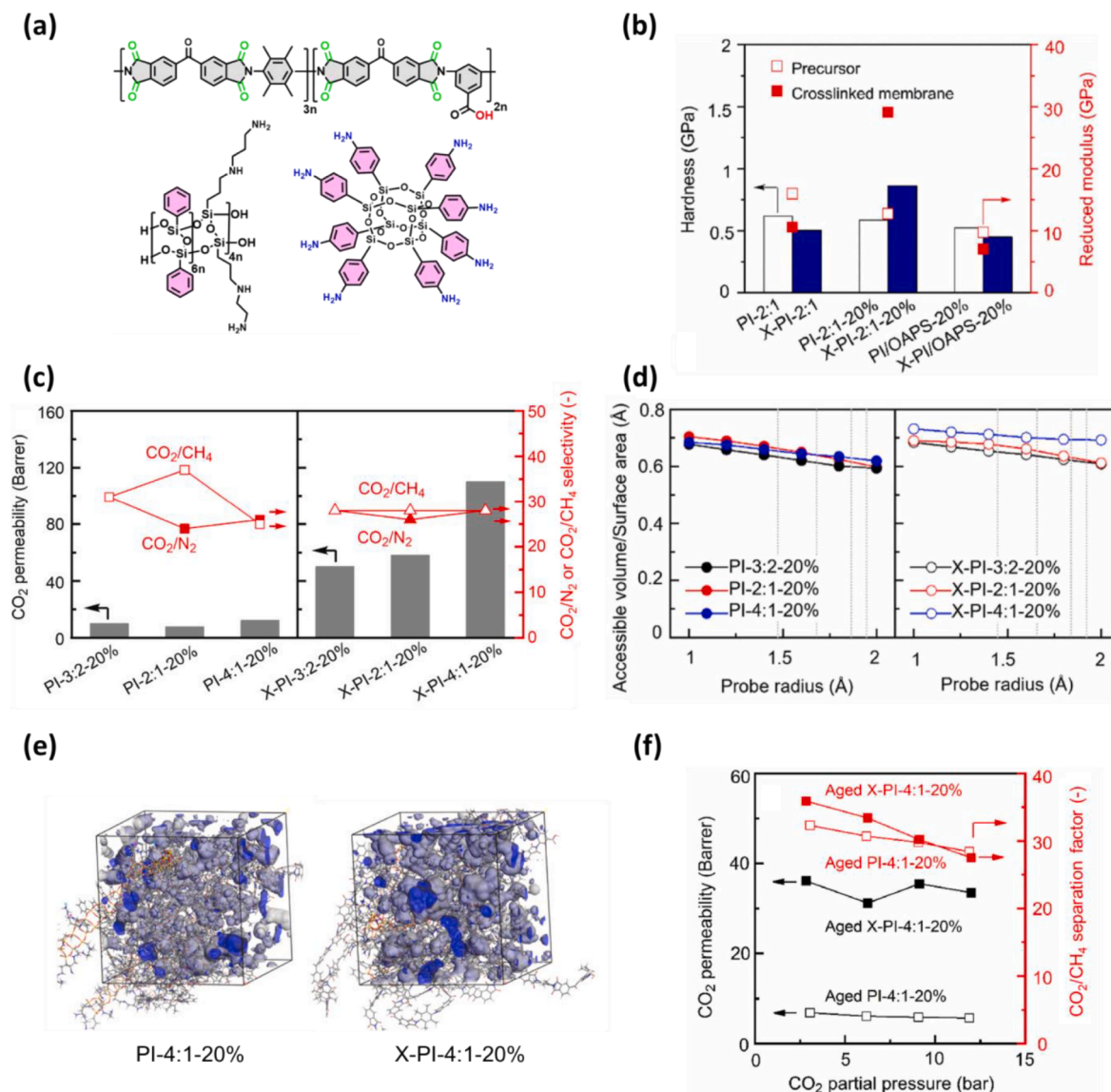
Fig. 14. (a) Chemical structures of BTDA-Durene:DABA, LPSQ, and OAPS, (b) mechanical properties of precursor membranes and cross-linked membranes derived from PI-2:1. (c) Single gas CO_2/N_2 and CO_2/CH_4 separation properties of hybrid precursors and hybrid cross-linked membranes. (d) The MD simulated accessible volume divided by the surface area of the membrane a function of the probe radius for hybrid PI/LPSQ and cross-linked X–PI/LPSQ membranes. (e) Free volume distribution in PI-4:1–20 % and X-PI-4:1–20 % membranes. Grey and blue colors represent the membrane's van der Waals surfaces and free volumes accessible for CO_2, respectively. (f) CO_2 permeability of aged PI-4:1–20 % and aged X-PI-4:1–20 % as functions of feed pressure at 35 °C measured with CO_2/CH_4 mixed gas. (Note: PI-x:y, where x and y are the ratios of Durene and DABA, respectively. PI-x:y-20 % refers to membranes with 20 wt% LPSQ introduced. X-PI-x:y refers to cross-linked PI/LPSQ membranes.) (Copyright from Ref. [69]).

yield mesoporous structures [23].

Recent advancements in pore structure engineering for silica membranes have introduced strategies such as templating and chemical modification. Organic templates—structure-directing agents—are incorporated into the sol to guide pore formation and subsequently removed by calcination. This allows tuning of pore diameter (typically 0.4–0.6 nm) and porosity. For instance, octyl aryl polyether alcohols have been shown to generate microporous networks, and the pore size can be modulated by adjusting the length of their polyoxyethylene chains [23]. Alternatively, chemical modification of the silica network using functionalized alkoxysilanes or bis-silyl precursors has been demonstrated to tailor pore architecture [24–26]. Precursors such as 1, 2-bis(triethoxysilyl)ethane ($(RO)_3Si–C_2H_4–Si(OR)_3$) introduce flexible bridging units that act as spacers in the silica framework, modifying the resulting pore structure and connectivity [80–82]. Moreover, incorporating alkoxysilanes bearing specific functional groups can enhance

affinity toward target gas molecules, thus improving separation performance. For instance, Yu et al. reported that incorporating sterically hindered amine groups into the silica network significantly increased CO_2 permeance by lowering the activation energy for CO_2 transport [83, 84].

Despite the excellent separation performance of sol-gel-derived microporous silica membranes, their stability under humid conditions remains a concern. Surface hydroxyl groups on silica can interact with steam, leading to network degradation at elevated temperatures. To address this limitation, metal doping strategies have been developed to enhance hydrothermal stability and gas transport properties. Nickel-doped silica membranes, for example, exhibit improved H_2 permeance and structural integrity over a wide temperature range (35–300 °C). Yoshida et al. attributed this to the reversible adsorption of hydrogen on nickel sites, which increases the density of active hydrogen transport pathways within the silica matrix [85]. Binary metal doping—such as
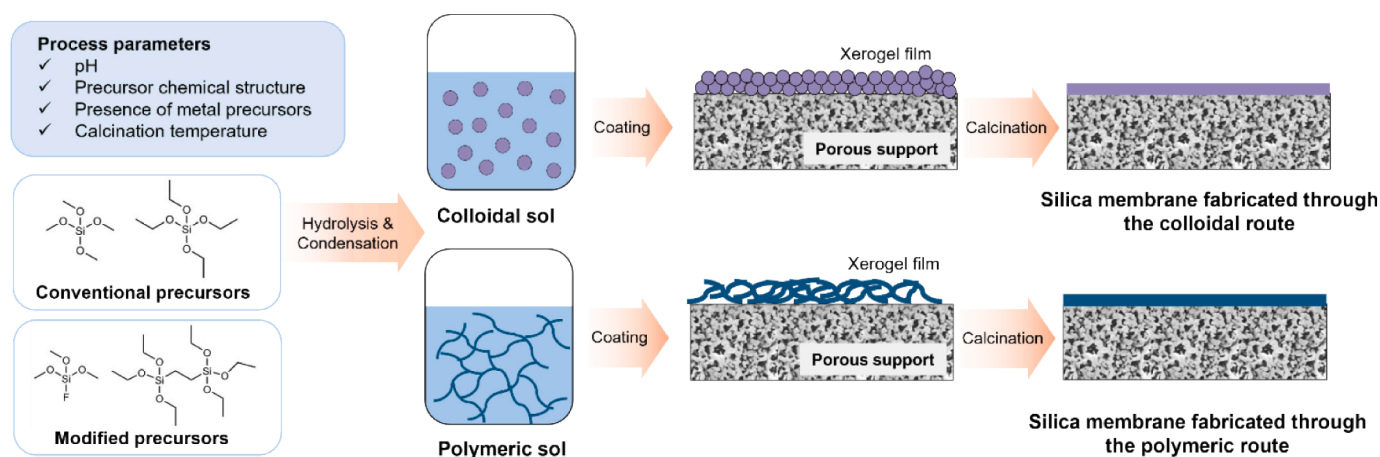
Fig. 15. Schematic illustration of the sol-gel process for preparing amorphous silica membranes, showing the distinction between the colloidal and polymeric routes.

Pd/Co [29] and La/Ni [30] combinations—via acid-catalyzed sol-gel routes has also been investigated. Notably, La/Ni co-doping was shown to suppress La–O–Si aggregation, maintaining a high degree of microporosity with an average pore size of 0.45 nm. The effect of metal doping is strongly influenced by the oxidation state and coordination environment of the dopants, which will be further discussed in Section 3.3.2.

Another effective approach to tailoring the pore structure of silica membranes is fluorine doping. Rana et al., demonstrated that adding NH₄F to the sol during synthesis introduces reactive fluorine, forming Si–F bonds that loosen the silica matrix and increase gas permeance [31]. Fluorine incorporation also reduces the concentration of hydrophilic Si–OH groups, thereby enhancing hydrothermal stability with increasing fluorine content. These effects enable improved performance under humid and high-temperature conditions. Further, the sol-gel method is relatively scalable via conventional techniques such as dip-coating. While scale-up has been demonstrated using closed-vessel and roll-to-roll systems, membrane-to-membrane reproducibility remains a challenge [86,87]. Overall, Fig. 15 summarizes the sol-gel fabrication of amorphous silica membranes and the key process parameters—such as catalyst type, calcination temperature, templating agents, and dopants—that can be tuned to optimize pore structure, gas separation efficiency, and stability.

3.2. CVD-derived silica membranes

CVD is a versatile technique for fabricating nonporous or microporous inorganic thin films. Unlike the sol-gel process, which involves colloidal or polymeric precursors, the molecular-scale precursors used in CVD enable deposition not only on external surfaces but also within meso- and macropores of porous substrates. This often results in denser silica networks with narrower pore size distributions, leading to higher gas selectivity and lower permeance compared to sol-gel-derived membranes [74]. Further, CVD typically produces ultrathin selective layers in the range of 20–30 nm. Deposition parameters can be finely tuned to achieve precise control over thickness and uniformity. CVD enables fabrication of membranes with highly uniform pore size distributions, typically centered around 0.3–0.5 nm, due to its vapor-phase precursor delivery and controlled reaction interface [25]. In a typical CVD process, an alkoxysilane precursor (e.g., tetraethoxysilane, TEOS, or tetramethoxysilane, TMOS) is vaporized and introduced into a reaction chamber along with a carrier gas (usually argon or nitrogen). Upon contacting a heated substrate in the presence of a reactive gas (e.g., O₂, air, or ozone), the precursor undergoes thermal decomposition, oxidation, or hydrolysis, leading to the formation of a silica film.

CVD-based membrane fabrication on porous substrates is generally classified into two main configurations based on precursor delivery: co-current CVD and counter-diffusion CVD. In co-current CVD, both precursor and reactive gases are introduced from the same side of the substrate, with a vacuum applied on the opposite side to minimize pinhole formation. Control over flow rate and composition allows tuning of deposition depth, although film growth is not self-limiting and can lead to excessive densification and reduced permeance. In counter-diffusion CVD, precursors and reactive gases are fed from opposite sides of the substrate. Deposition occurs where the two gases meet within the pores, forming a silica layer that self-limits as the pore throat narrows below the precursor size. This configuration enables fine control of film thickness and pore size: smaller precursors form denser, more selective membranes, while bulkier ones result in larger pores and reduced selectivity [88]. Compared to co-current CVD, the counter-diffusion method generally produces membranes with higher gas permeance and better structural precision due to its self-limiting deposition behavior.

While conventional thermal CVD processes operate at temperatures above 300 °C, limiting precursor selection and substrate compatibility, plasma-enhanced chemical vapor deposition (PECVD) enables film formation at significantly lower temperatures. In PECVD, plasma-activated carrier gases promote the reaction of vapor-phase alkoxysilanes, allowing for the incorporation of functionalized precursors and the fabrication of organosilica membranes with enhanced thermal stability and tunable hydrophobicity. For example, Nagasawa et al. [27,28] demonstrated the fabrication of polymer-supported silica membranes via a two-step atmospheric-pressure PECVD process (Fig. 16). First, a polysiloxane-like layer was deposited to provide uniform surface coverage. Although this layer exhibited lower selectivity due to its relatively open network, it ensured continuous coating. Next, a dense silica-like layer was deposited to enhance selectivity but often suffered from poor uniformity when applied alone. By sequentially stacking the two layers, the researchers successfully produced a defect-free composite membrane that combined high selectivity with good structural integrity.

Although CVD offers excellent structural precision, it requires more complex and costly equipment compared to sol-gel processes. However, advancements such as plasma-enhanced CVD (PECVD) and atmospheric pressure PECVD (AP-PECVD) have enabled scalable fabrication on low-cost polymeric supports under ambient conditions [27,28]. Notably, the counter-diffusion CVD configuration has shown superior reproducibility compared to sol-gel methods, which often suffer from variability due to sol preparation, coating uniformity, and drying dynamics [89].
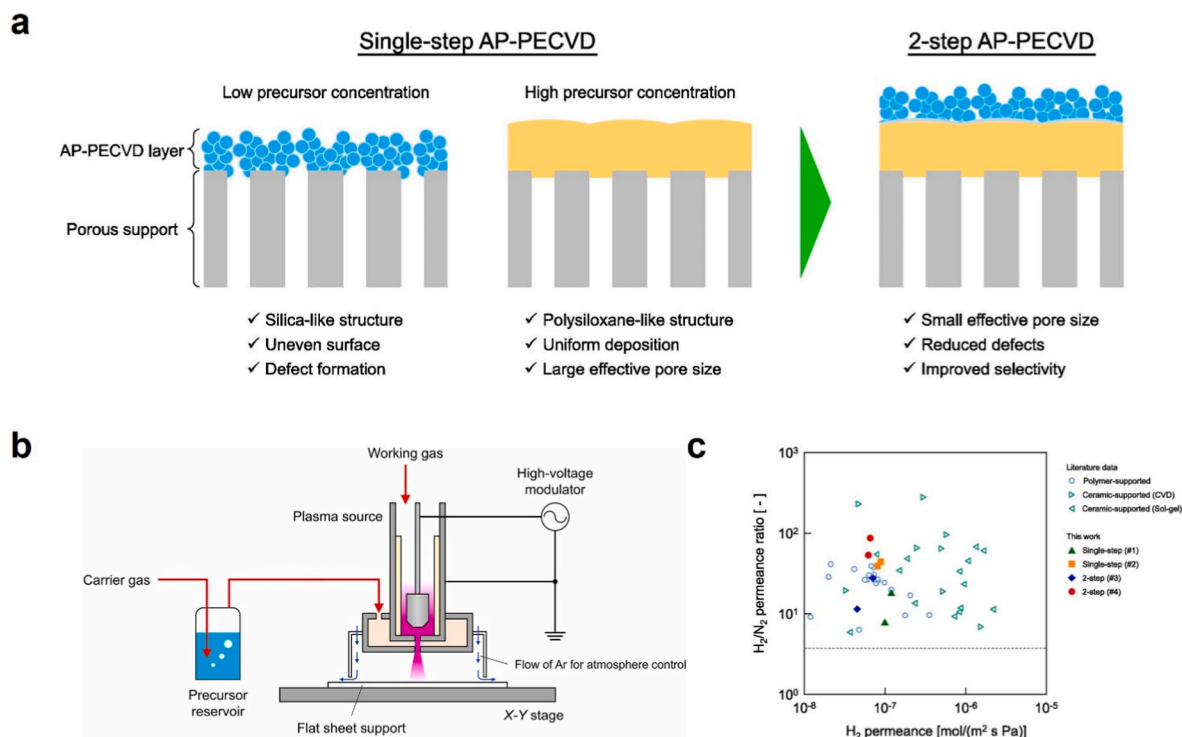
Fig. 16. (a) Schematic image of the two-step AP-PECVD process, (b) illustration of the AP-PECVD system (Copyright from Ref. [27]) (c) H_2/N_2 separation performance of AP-PECVD-derived membranes (Copyright from Ref. [28]).

3.3. Effect of synthesis parameters on pore architecture and gas transport

3.3.1. Gas transport mechanisms in silica membranes

In silica membranes with sub-nanometer pore sizes, the dominant gas transport mechanism is highly dependent on the pore diameter. When the pore size is smaller than approximately 0.4 nm, gas transport primarily follows the solution-diffusion mechanism. In this regime, gas molecules dissolve into the membrane material and then diffuse through it. Bighane et al. demonstrated that silica membranes prepared via oxidative thermolysis of polydimethylsiloxane exhibited solution-diffusion behavior rather than Knudsen diffusion, as evidenced by their high gas selectivity [90,91]. As pore size increases beyond the kinetic diameter of gas molecules but remains within the microporous range, a partial transition occurs toward the gas translation (GT) mechanism [92,93]. The GT model assumes that gas molecules move between adsorption sites via translating through pores larger than the penetrant size, overcoming energy barriers present in the channels between these sites. This translational movement is thermally activated and resembles Knudsen diffusion but incorporates molecular-level energy barriers, making it more accurately described as activated Knudsen diffusion. The GT mechanism accounts for potential energy fields within the pores and interactions between the gas molecules and pore surfaces. These gas-wall interactions become increasingly significant as the pore size approaches the kinetic diameter of the penetrant, particularly for gases with high polarizability such as CO_2. [93]. In such cases, deviations from Knudsen behavior are often observed and must be accounted for using models that include activation energies and adsorption potentials. For instance, Yoshioka et al. employed a dual control plane–non-equilibrium molecular dynamics (DCP-NEMD) approach to investigate gas permeation through amorphous silica membranes with micropores of approximately 6 Å or 8 Å in diameter [94]. Their study revealed that stronger gas-pore wall interactions led to enhanced gas permeance and a more significant temperature dependence of permeation. These effects were attributed to the depth of the attractive potential wells within the pores, which varied according to

pore size and gas properties. In summary, the gas transport mechanism in silica membranes transitions from solution-diffusion to gas translation or activated Knudsen diffusion as the pore size increases. Understanding the nature of gas-pore wall interactions and their dependence on synthesis conditions is essential for accurately modeling transport and optimizing membrane performance.

Beyond single-gas transport, mixed-gas feeds introduce complexities such as competitive adsorption. Hassan et al., reported on this effect while investigating the separation performance of silica hollow fiber membranes under binary O_2/N_2 and CO_2/CH_4 mixtures [95]. Under 373 K, mixed-gas selectivities were up to 20 % higher than single-gas selectivities. This was attributed to the more strongly interacting species saturating adsorption sites and impeding the transport of the weakly interacting species. Above 373 K, however, the mixture and single-gas selectivities were equal, suggesting that competitive adsorption effects were negligible at higher temperatures.

3.3.2. Effect of synthesis parameters on the pore architecture of silica membranes

The pore structure and gas separation performance of silica membranes are strongly influenced by synthesis parameters such as pH conditions, calcination temperature, the use of templating agents in sol-gel processes, and deposition conditions in CVD. In sol-gel-derived membranes, the choice of catalyst significantly affects the resulting porosity. Acidic conditions promote hydrolysis and the formation of long, linear chains, yielding microporous structures. In contrast, basic conditions lead to highly condensed networks and larger particle agglomerates, resulting in mesoporous architectures. For example, silica membranes synthesized via acid-catalyzed hydrolysis of TEOS exhibited a porosity of 54 % with pore diameters ranging from 1 to 5 nm, whereas base-catalyzed synthesis yielded membranes with 70 % porosity and broader pore diameters of 1–20 nm [23]. Calcination temperature also plays a pivotal role in tuning the pore size and membrane stability. Optimized calcination conditions have produced sol-gel-derived membranes with exceptional H_2/CH_4 and H_2/N_2 selectivity, achieving He

and H_2 permeances of 8.6 x 10^{-7} and 5.5 x 10^{-7} mol m^{-2} s^{-1}·Pa^{-1}, respectively, and selectivities of up to 2350 (He/CH$_4$) and 1500 (H$_2$/CH$_4$) at 500 °C [92,96]. High-temperature calcination (e.g., 700 °C) was shown to further densify the siloxane matrix, improving the membrane's ability to exclude water vapor while maintaining separation performance, which showed steady H$_2$/CH$_4$ selectivities around 110, with improved exclusion of water vapor at higher calcination temperatures due to densification of the siloxane matrix [97]. Qi et al. reported that increasing the calcination temperature from 300 °C to 450 °C led to reduced gas permeance and improved He/CO$_2$ and H$_2$/CO$_2$ selectivity in Nb-doped hybrid silica membranes [98]. However, calcination at 500 °C caused structural degradation due to the thermal cleavage of the –Si–CH$_2$–CH$_2$–Si– linkage, resulting in a shift toward Knudsen-type diffusion. Interestingly, Kanezashi et al. observed that for membranes synthesized using triethoxyfluorosilane (a fluorine-modified precursor), the gas separation performance remained largely unaffected by calcination temperature due to suppression of densification by the fluorine moiety [96].

Templating approaches further allow control over micropore structures. For instance, nonionic surfactants such as octyl aryl polyether alcohols can be introduced into the sol to guide pore formation through self-assembly. The chain length of the surfactant significantly impacts the resulting membrane architecture: increasing the polyether chain length (X) widened the pore size distribution and increased the average pore size. Additionally, raising the surfactant/TEOS ratio from 0.16 to 0.55 increased the mean pore size from 3.2 Å to 3.7 Å and porosity from 20.9 % to 35.5 % [75].

In CVD-derived membranes, deposition conditions such as time, temperature, gas atmosphere, and configuration play critical roles in determining pore size and distribution—from ultra-microporous to mesoporous regimes [88]. Ha et al. investigated the impact of deposition time at various temperatures (200 °C, 400 °C, and 600 °C) and observed that increasing deposition time decreased H$_2$ permeance while increasing H$_2$/N$_2$ selectivity, primarily due to pore plugging. At 600 °C, complete pore sealing occurred within 30 min; at 400 °C, it required more than 2 h; and at 200 °C, pore plugging was incomplete even after 70 h, resulting in low selectivity [99]. The deposition atmosphere also plays a role. Silica films deposited in the presence of oxygen were denser and exhibited lower gas permeance than those formed in oxygen-free environments. Although the detailed mechanism remains unclear, this suggests that oxygen facilitates silica network densification. Finally, the CVD reactor configuration can impact membrane performance. Using a crossflow configuration instead of a co-current setup significantly improved separation properties, achieving a H$_2$ permeance of 2.8 x 10^{-7} mol m^{-2} s^{-1}·Pa^{-1} and H$_2$/N$_2$ selectivity greater than 2000 at 500°C—approximately nine times higher than the membrane fabricated using co-current flow [100,101].

Silica membranes synthesized with organosilane or organically-bridged precursors—via either sol-gel or plasma-enhanced CVD methods—exhibit pore structures that differ significantly from those fabricated without such organic moieties. Li et al. reported that membranes derived from methyltriethoxysilane and phenyltriethoxysilane exhibited larger pore sizes (5.2 Å and 7.6 Å, respectively) than those synthesized from triethoxysilane (3.4 Å), as determined by normalized Knudsen-based permeance (NKP) measurements. This increase in pore size was attributed to steric hindrance from pendant organic groups, a lower degree of cross-linking, and nano-scale aggregation of hydrophobic groups. However, the increase in pore size did not correspond to enhanced gas permeance due to a reduction in effective free volume, as bulky pendant groups partially obstructed transport pathways [102]. In contrast, the use of bridged silane precursors such as bis(triethoxysilyl) ethane (BTESE) resulted in more open network structures compared to conventional triethoxysilane-derived membranes. Guo et al. further demonstrated that silica membranes prepared from bridged biphenyl precursors exhibited a substantial increase in CO$_2$ permeance—from 1087 GPU to 5465 GPU—accompanied by a decrease in CO$_2$/N$_2$

selectivity from 30 to 13, compared to membranes derived from precursors with phenyl pendant groups [79]. These findings suggest that the gas transport properties of phenyl-functionalized silica membranes are more dependent on the positional configuration of the phenyl groups within the network than by interactions induced by their chemical affinity.

Incorporation of metal dopants into silica matrices has also been shown to significantly influence pore characteristics and gas transport behavior. Miller et al. demonstrated that the gas separation performance of cobalt oxide-doped silica membranes depends strongly on the redox state of the dopant [103]. Upon exposure to hydrogen, Co$_3$O$_4$ was reduced to Co(OH)$_2$ and CoO, causing volume expansion of the embedded particles. This expansion widened narrow bottlenecks in the silica network, reducing gas selectivity. As a result, the H$_2$/N$_2$ selectivity decreased markedly with increasing temperature—from 50 at 200 °C to just 12 at 450 °C. Similarly, Anggarini et al. investigated the effects of reduction on silver-doped aminosilica membranes [104]. Using a high silver-to-amine ratio (0.5), they observed increased microporosity, surface area, and pore volume. Spectroscopic analysis revealed that Ag$^+$ ions bonded to amine groups during hydrolysis and condensation, followed by in-situ reduction to Ag^0 nanoparticles. These silver particles enhanced the diffusion of small molecules (e.g., H$_2$), while the amorphous silica framework effectively excluded larger species. As a result, the membrane exhibited a high H$_2$ permeance of 1.46 x 10^{-6} mol m^{-2} s^{-1}·Pa^{-1} and exceptional H$_2$/C$_3$H$_8$ selectivity of 1500, significantly outperforming unmodified counterparts (selectivity ~ 100).

Bimetallic doping strategies have recently emerged as a promising route to improve hydrogen separation through synergistic effects between metal species, which tune both hydrogen activation and pore morphology. For instance, La–Ni co-doped silica membranes demonstrated more uniform metal dispersion and a refined microporous network, leading to a fivefold enhancement in H$_2$/N$_2$ selectivity and a H$_2$ permeance of 1.86 x 10^{-7} mol m^{-2} s^{-1}·Pa^{-1}, surpassing the performance of single-metal-doped membranes [30]. In another study, Ballinger et al. showed that dual doping with palladium and cobalt enhanced gas permeance following reduction [29]. Specifically, the reduction of PdO to metallic Pd created molecular gaps (Fig. 17a), increasing pore volume (Fig. 17b), while cobalt oxide domains remained structurally stable due to their lower reducibility. However, this increase in free volume came at the expense of selectivity: He/N$_2$ and He/CO$_2$ selectivities decreased from 70 to 30 and 40 to 15, respectively. These findings underscore the structural tunability offered by bimetallic doping, though such modifications must be balanced against potential trade-offs in selectivity. It is important to note that hydrogen activation behavior in bimetallic systems is highly sensitive to operating conditions and metal identity [32]. For instance, Mg–Ni composites require elevated temperatures (200–300 °C) and high pressure (12 bar) to optimize hydrogen uptake [33]. Such observations highlight the need for continued research into structure-property relationships in metal-doped silica membranes to enable rational design of high-performance materials for selective gas separations. To place these efforts in a broader context, Fig. 18 summarizes the H$_2$/N$_2$ and CO$_2$/CH$_4$ separation performance of representative silica membranes reported in literature, comparing them with polymeric membranes [27–30,77,97, 105–123,132].

4. Comparative analysis

4.1. Performance trends across the Si–O structural continuum

Silicon–oxygen (Si–O) frameworks span a structural continuum from fully inorganic amorphous silica to organic–inorganic hybrids such as polysiloxanes and polysilsesquioxanes. Amorphous silica membranes derive their separation performance primarily from molecular sieving within the rigid Si–O–Si network, making them well-suited for high-temperature hydrogen separation. However, their brittleness and
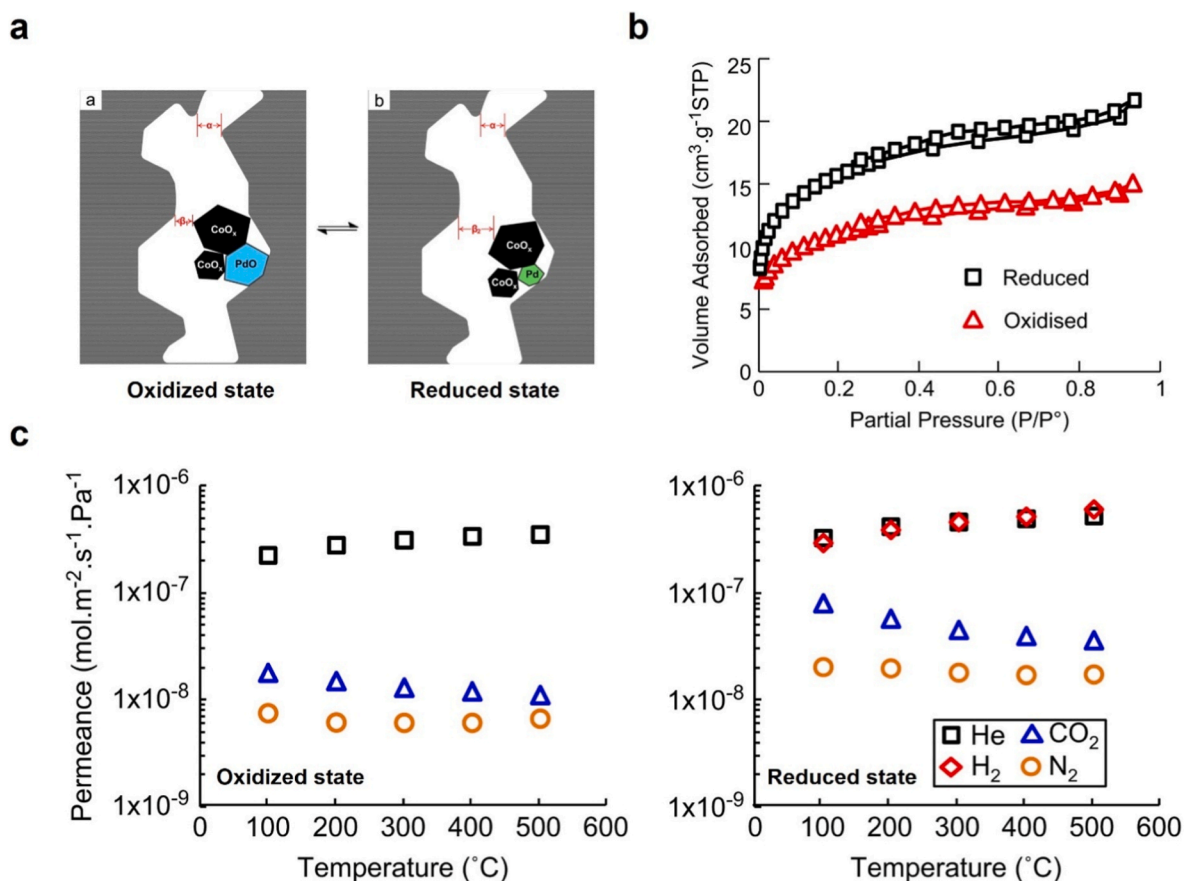
Fig. 17. (a) Representation of the change in porosity due to interaction between cobalt oxide and palladium metal/oxide for the oxidized and reduced membrane. (b) N_2 adsorption isotherms of reduced and oxidized xerogels. (c) Single gas permeance of the oxidized and reduced PaCo-doped silica membrane (Copyright from Ref. [29]).

hydrothermal instability limit large-scale deployment. At the opposite end of the spectrum, polysiloxanes possess flexible, loosely packed Si–O backbones, resulting in high permeability and transport dominated by solubility effects rather than strict size exclusion. This makes them effective for separating larger or more condensable gases, although their relatively low selectivity often necessitates modification via crosslinking or inorganic fillers.

PSQs occupy an intermediate position, combining inorganic network rigidity with tunable organic functionality. The choice of pendant groups can modulate free volume, polarity, and gas-polymer interactions, thereby enhancing permeability, selectivity, stability, and resistance to plasticization. Furthermore, the dimensional architecture of PSQs—such as cage, ladder, or chain structures— affects gas transport properties. LPSQs, in particular, with their high aspect ratios, have shown higher CO_2 permeability after crosslinking than POSS, suggesting that the ladder-like architecture is more favorable for enhancing CO_2 permeability. Understanding these structure-property relationships across the Si–O continuum enables the rational design of membranes tailored for specific gas separation applications.

However, despite these advantages, PSQ-based membranes still face several challenges, including limited hydrothermal stability and difficulties in achieving uniform dispersion at higher loadings. Filler aggregation at elevated concentrations can result in structural defects, diminished gas permeability, and compromised selectivity. These drawbacks underscore the need for further innovations in surface functionalization, polymer-filler interactions, and membrane processing techniques to realize the full potential of PSQ-based systems in practical gas separation applications. To clarify the comparative performance and practical considerations of these two membrane classes, Table 2

provides a side-by-side summary of fabrication methods, gas separation performance, and stability characteristics.

4.2. Approaches to address membrane challenges

4.2.1. Organic-inorganic composite membranes

Polymeric membranes are attractive for gas separation due to their ease of fabrication and low production cost. However, their commercial deployment is hindered by the inherent permeability-selectivity trade-off, susceptibility to plasticization, and physical aging. Incorporating PSQs into polymer matrices has emerged as an effective strategy to address these limitations. Table 1 summarizes reported effects of PSQ incorporation across various polymer systems, highlighting how PSQ loading influences membrane performance. At low concentrations, PSQs—including POSS—disrupt polymer chain packing, increase free volume, and enhance gas permeability, even in the absence of strong PSQ-polymer interactions. At higher loadings, however, PSQs tend to aggregate, reducing permeability and sometimes compromising selectivity. No universal correlation between gas separation performance and POSS-polymer interaction strength has been observed, indicating that dispersion and morphology control are critical.

Beyond blending, copolymerization enables the direct integration of POSS units into polymer backbones, producing stable hybrid membranes with finely tunable properties. By controlling monomer composition and sequence, block copolymers have been synthesized that retain the intrinsic permeability of POSS while preserving the selectivity of the host polymer. This synergistic effect allows for substantial performance enhancement without sacrificing stability.

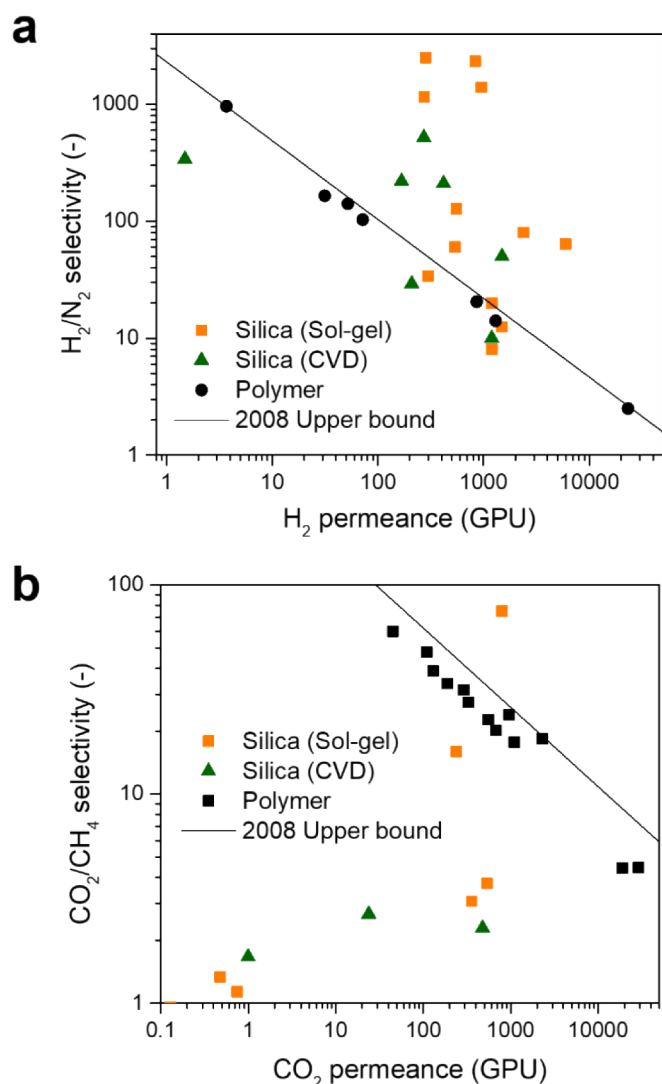Cross-linking offers an even greater potential for performance

Fig. 18. Separation performance comparison between amorphous silica and polymeric membranes. (a) H_2/N_2, (b) CO_2/CH_4.

improvement. While POSS addition via blending or copolymerization disrupts chain packing and boosts permeability, cross-linking—particularly with LPSQs—leverages their high aspect ratio and pseudo-2D structure to create highly interconnected pore networks. This architecture can yield CO_2 permeability up to $16 \times$ higher than the pristine membrane while maintaining selectivity. As illustrated in Fig. 19, a cross-linked LPSQ composite (red star) far exceeds the performance of a simple blend (grey circle). In addition to higher permeability, LPSQ-based cross-linked membranes demonstrate superior mechanical robustness and plasticization resistance compared to POSS-based analogues, owing to the rigidity and structural stability of the LPSQ siloxane framework.

4.2.2. Amorphous silica membranes

Due to their high H_2/N_2 and CO_2/CH_4 selectivities at high temperatures, silica membranes are promising candidates for harsh industrial processes such as steam reforming and the water-gas shift (WGS) reaction, where polymer membranes typically fail. Although their fabrication cost remains higher, commercial application is feasible once critical issues such as hydrothermal stability and scalability are resolved. However, long-term mixed-gas performance data under realistic process conditions are scarce, limiting industrial translation.

Hydrothermal stability remains one of the most critical challenges

Table 2

Comparative summary of representative gas transport performance, fabrication methods, and stability characteristics of PSQ-based hybrid and amorphous SiO_2 membranes. PSQ hybrids offer tunable free volume and processability, while amorphous SiO_2 membranes provide superior thermal and hydrothermal stability with intrinsic molecular sieving.

Property	PSQ-based hybrid membranes	Amorphous SiO2 membranes
H_2 permeability	Limited reports	1000-6000 (GPU) ($\approx 3 \times 10^4$-1.8×10^5 Barrer)
CO_2 permeability	50-14000 (Barrer)	150-800 (GPU) ($\approx 2.5 \times 10^3$-2.6×10^4 Barrer)
H_2/N_2 selectivity	Limited reports	20–2500
CO_2/CH_4 selectivity	5–40	1–140
Fabrication Method	Blending/Copolymerization/Cross-linking with POSS or LPSQ	Sol-gel (acid/base catalyzed), CVD, PECVD
Hydrothermal stability	Limited reports	Fluorine- or metal-doped systems and organically bridged systems show hydrothermal stability up to 600 °C
Scalability/Mechanical robustness	Potentially flexible and solution-processable Few large-scale demonstrations	Brittle, limited scalability Needs ceramic supports
Advantages	Tunable free volume and surface polarity Mitigates plasticization and aging Mechanically flexible	High thermal & chemical stability Precise molecular sieving Stable under harsh gas conditions
Disadvantages	Limited thermal stability Performance variation by filler dispersion Long-term data scarce	Brittle, hydrothermal degradation in steam Costly fabrication
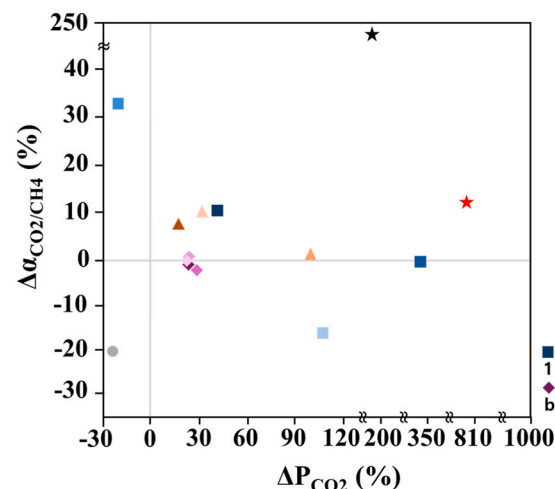
Fig. 19. Percentage changes in CO_2/CH_4 selectivity and CO_2 permeability from pristine membranes to their optimal composite counterparts. Symbols (numerical and alphabetical) correspond to the chemical species listed in Table 1.

for silica membranes operating under steam-rich environments common in H_2-producing reactions. Steam exposure leads to hydrolysis of Si–O–Si bonds into silanols (Si–OH), resulting in micropore collapse, macropore coarsening, and degradation of permeability, selectivity, and mechanical strength [122–124]. Even metal-doped membranes are not fully immune; for instance, Kanezashi and Asaeda reported that the H_2 permeances of Ni-doped silica membranes decreased to one-tenth of its initial value after 38 h of steam exposure [35]. Mitigation strategies include both inorganic and organic modifications. Metal doping with elements such as Nb, Ni, and Al has demonstrated enhanced stability

[34–36]. A hydrothermal pre-treatment of Ni-doped membranes at 500 °C was shown to suppress densification during operation, limiting H_2 permeance loss to 40 % after 60 h [35].

Incorporation of organic linkages or hydrophobic groups also improves stability by minimizing water adsorption and pore structure collapse [125,126]. For instance, Wei et al. reported that silica membranes derived from a mixture of (trifluoropropyl)triethoxysilane (TFPTES) and TEOS maintained stable H_2/CO_2 separation performance for 220 h under mixed-gas conditions with steam at 200 °C [126]. Similarly, fluorine-doped silica membranes exhibited excellent durability between 200 and 300 °C due to reduced silanol formation [31]. Hybrid organosilica membranes prepared from bis(triethoxysilyl)ethane (BTESE) also showed superior hydrothermal stability compared to pure silica (TEOS) membranes, retaining performance after 300 °C treatments, while TEOS-derived silica suffered irreversible degradation [127]. This improvement is attributed to enhanced hydrophobicity, increased network connectivity, and reduced flexibility of the silica framework [128]. Furthermore, ten Hove et al. demonstrated that Zr-doped BTESE membranes exhibited stable gas permeance under a simulated WGS feed (2 bar, 200 °C), showing only an initial 40 % decrease within the first hour, followed by stabilization over extended operation [127].

Despite promising performance characteristics, several critical barriers remain for the **industrial deployment** of silica membranes, particularly related to **scale-up, durability**, and **economic viability.** While precursor materials such as TEOS are inexpensive, fabrication of **ultrathin selective layers (<100 nm)** over large areas remains technically challenging. These thin layers are prone to **defects** such as pinholes or cracks induced by dust contamination, support roughness, or mechanical stresses during handling or thermal cycling [129]. To address these issues, both **process innovations** and **material modifications** have been proposed. For example, **Luiten et al.** demonstrated a **closed-vessel coating system** for the inner surface of 55 cm-long tubular supports, yielding membranes with high H_2 permeance (1500–2980 GPU) and H_2/CH_4 selectivity of 350–400 [87]. On the materials side, **boron oxide doping** has been shown to **reduce the hardness and Young's modulus** of silica membranes, increasing mechanical flexibility and helping to prevent crack formation during thermal treatment [129].

In terms of **long-term stability**, recent demonstrations are encouraging. **Yacou et al.** reported the fabrication and operation of a **CoOxSi-based silica membrane module** with an effective area of **545 cm²**, which maintained consistent H_2 permeance at 500 °C under repeated thermal cycling conditions [86]. Such studies confirm the technical feasibility of scaling up silica membranes while retaining performance over extended use. Nonetheless, for broader adoption, future research must focus on **cost-effective manufacturing, improved reproducibility**, and **module integration strategies**, particularly for large-area flat-sheet or hollow fiber formats compatible with industrial gas separation systems. In summary, silica membranes show strong potential for high-temperature and steam-containing processes; however, systematic evaluation under high-pressure CO_2 exposure is still lacking. Future studies should address this gap to validate the feasibility of silica-based membranes for broader high-pressure industrial applications.

4.3. Hybrid strategies that bridge PSQs and amorphous silica

Hybrid membrane designs that integrate PSQs with amorphous silica combine the complementary strengths of both materials: the high thermal, chemical, and mechanical stability of amorphous silica networks with the tunable flexibility, organic functionality, and enhanced free volume of PSQ-based frameworks. These hybrids aim to simultaneously improve permeability, selectivity, and long-term durability under industrial separation conditions.

A widely studied strategy is the sol–gel co-condensation of conventional silica precursors—such as TEOS or TMOS—with organosilane precursors featuring covalent Si–C–Si bridges, including BTESE or bis (triethoxysilyl) methane (BTESM) [80,81]. This bimodal precursor system yields a homogeneous hybrid network in which rigid Si–O–Si siloxane bonds from amorphous silica are interlinked with flexible organic bridges derived from PSQs. At the molecular-level, the organic linkages act as "molecular spacers", loosening the dense silica matrix and slightly enlarging the pore size. These hybrid networks often exhibit enhanced hydrothermal stability compared with pure silica, attributed to their high density of reactive groups, which promote a strongly crosslinked structure [81,130–132]. Gas separation studies indicate that increasing the number of carbons in the bridging unit raises H_2 and CO_2 permeance, through typically at the expense of selectivity (e.g., H_2/N_2, H_2/CH_4) [82].

Another strategy involves modifying the silica network by direct incorporation of octabenzamidopropyl-functionalized POSS into a BTESE-derived silica matrix [133]. Although BTESE and POSS do not undergo cross-linking reactions, up to 66.7 % POSS content was successfully introduced into the membrane. Increasing the POSS content led to reduced permeance for H_2, CO_2, and N_2, while H_2/N_2 selectivity increased by 160 %. The authors attributed this to the long alkyl chains in POSS, which reduced the effective pore volume and hindered gas transport, as evidenced by the decline in CO_2 adsorption capacity with increasing POSS concentration. A further approach involved the fabrication of silica membranes via sol-gel condensation using POSS precursors [134]. POSS-derived silica membranes calcined at 300 °C exhibited looser network structures than those derived from TEOS, resulting in a high H_2 permeance (5970 GPU) and moderate H_2/N_2 selectivity (20) at 200 °C. This behavior was attributed to the formation of large intercubic pores through Si–O–Si cross-linking between POSS units. Upon increasing the calcination temperature, the H_2 permeance decreased (2690 GPU), while H_2/N_2 selectivity increased significantly (*ca.* 130), indicating densification of the silica network and improved molecular sieving capability.

5. Summary and future perspectives

PSQ-based composite membranes represent a versatile platform for overcoming key limitations of conventional polymeric membranes—namely the permeability-selectivity trade-off, plasticization under high-pressure condensable gases, and physical aging. These membranes can be fabricated via blending, copolymerization, or cross-linking, with performance enhancements arising not from gas transport through the inherently impermeable PSQ cages, but from their ability to disrupt polymer chain packing, increase free volume, and facilitate molecular diffusion. Among these approaches, thermal cross-linking of polyimides with LPSQs has proven particularly effective. The high aspect ratio and rigid double-stranded siloxane architecture of LPSQs promote the formation of large, interconnected pore networks during cross-linking, leading to substantial permeability gains while preserving selectivity. LPSQs also impart mechanical reinforcement, enhance resistance to plasticization by rigidifying polymer chains, and mitigate non-equilibrium relaxation, thus reducing aging-related performance losses. Gas separation performance is strongly influenced by FFV, which depends on interchain distances and chain mobility; phenyl-functionalized LPSQs, for instance, improve modulus and hardness while maintaining favorable transport properties. Despite these advantages, systematic studies on structure–property relationships in LPSQ-based membranes remain limited, underscoring the need for deeper mechanistic understanding.

Amorphous silica membranes, prepared primarily by sol-gel or CVD, offer complementary advantages: precise molecular sieving, high thermal stability, and tunable pore structures. Their gas separation performance can be tailored through synthesis parameters such as pH, calcination temperature, doping with metals or fluorine, which influence pore size distribution, hydrothermal stability, and selectivity. Hybrid silica membranes that incorporate Si–C–Si bridged organosilane

precursors combine the rigidity of Si–O–Si backbones with the flexibility and stability of organic linkers. These molecular spacers relax the dense silica network, increasing pore accessibility and improving H_2 and CO_2 permeance, while longer bridging groups enhance hydrothermal stability.

Looking forward, the rational design of hybrid architectures that bridge PSQs and amorphous silica offers a promising pathway to next-generation membranes that unify high permeability, selectivity, and long-term stability under industrial conditions. Emerging hybridization strategies should focus on constructing precisely controlled architectures, such as co-networks or interpenetrating polymer-silica systems, to combine the processability of PSQs with the rigidity and selectivity of amorphous SiO_2. For instance, incorporating POSS as a nanofiller into an organosilica matrix (e.g., BTESE) has been shown to reduce pore size and improve H_2/N_2 selectivity by up to 160 % compared to BTESE membranes alone [133]. Further control can be achieved through precursor blending, integrating rigid bridging groups into otherwise flexible chains to tune free volume and suppress pore collapse or blocking. Rational design of such hybrid systems will benefit from systematic exploration of LPSQ backbone modifications, alternative bridging motifs, and crosslinking chemistries to modulate chain packing, interfacial compatibility, and gas transport behavior. Realizing these structurally tailored hybrid systems require advanced characterization and modeling approaches. Operando techniques such as in situ FTIR, XAS, environmental TEM now enable direct observation of molecular-scale structural evolution under real operating conditions, offering insights into pore collapse, densification, or chemical degradation. In parallel, machine-learning-assisted design can accelerate membrane optimization by integrating high-dimensional datasets (e.g., composition, structure, performance) to predict structure-property relationships and guide precursor selection or synthesis conditions. The synergy between operando diagnostics and ML-guided modeling provides a powerful platform for designing robust, high-performance membranes tailored for complex industrial environments.

From a scalability perspective, future work should address the cost and integration challenges associated with silica membranes. In particular, low-temperature coating techniques compatible with porous polymer supports (e.g., AP-PECVD, solution infiltration) offer a route toward commercially viable spiral-wound or hollow fiber modules. Moreover, while many studies report promising short-term performance, long-term testing under humid, high-pressure, and mixed-gas conditions remains scarce. Stability under these realistic process environments—particularly for CO_2-containing or condensable gas feeds—is essential to demonstrate industrial relevance. Closing this gap is critical for the successful deployment of PSQ-silica hybrids and amorphous silica membranes in commercial gas separation processes.

Moreover, these two membrane platforms are well suited for distinct industrial operating regimes. PSQ-based membranes, which offer tunable free volume, chemical functionality, and resistance to CO_2-induced plasticization, are particularly promising for low-to-moderate-pressure separations, especially post-combustion CO_2 capture. Their demonstrated plasticization resistance also suggests potential for higher-pressure applications, although long-term stability validation remains necessary. In contrast, amorphous and Si–C–Si hybrid silica membranes exhibit exceptional thermal and hydrothermal stability, narrow pore size distribution, and robust molecular sieving capabilities, making them strong candidates for high-temperature separations, including: H_2 purification from reformate gases in water–gas shift reactors, ammonia cracking for hydrogen production, and exhaust steam upgrading in iron and steel manufacturing processes. Clarifying these application domains allows for a more strategic alignment between membrane material design and realistic process conditions, moving beyond material-centric metrics toward deployment-driven membrane engineering.

While continued progress in molecular-level membrane design remains essential, future research should also focus on interdisciplinary integration to maximize the functional utility of silica-based membranes. Once key requirements such as hydrothermal stability, scalability, and long-term durability under humid and high-pressure conditions are addressed, these membranes can play an enabling role in reactive separation systems. In particular, integration with membrane reactors offers exciting opportunities to simultaneously drive chemical reactions and selectively remove target products—enhancing both conversion efficiency and energy savings. Moreover, coupling silica-based membranes with electrochemical gas separation systems (e.g., for CO_2 or H_2) or photocatalytic CO_2 conversion platforms could yield compact, multifunctional devices for sustainable gas processing. These interdisciplinary applications require close collaboration between materials scientists, chemical engineers, and catalysis experts to co-design membranes that meet performance demands under dynamic process conditions. The convergence of materials innovation with process intensification and system-level engineering will be key to realizing next-generation membrane technologies for carbon capture, hydrogen production, and green chemical synthesis.

CRediT authorship contribution statement

Hyo Jung Kim: Writing – review & editing, Writing – original draft, Validation, Methodology, Investigation, Conceptualization. **Mohamed Gamal Mohamed:** Writing – review & editing, Writing – original draft, Investigation. **Hyun Jung Yu:** Writing – review & editing, Writing – original draft, Investigation. **Seo Hyeon Baek:** Writing – review & editing, Conceptualization. **Iqubal Hossain:** Writing – review & editing. **Shiao-Wei Kuo:** Writing – review & editing, Writing – original draft, Supervision, Methodology, Investigation, Conceptualization. **Jong Suk Lee:** Writing – review & editing, Writing – original draft, Supervision, Methodology, Investigation, Funding acquisition, Conceptualization.

Declaration of competing interest

The authors declare that they have no known competing financial interests or personal relationships that could have appeared to influence the work reported in this paper.

Acknowledgements

Data availability

Data will be made available on request.

References

[1] R. Spillman, Chapter 13: economics of gas separation membrane processes, in: Membrane Science and Technology, Elsevier, 1995, pp. 589–667, https://doi.org/10.1016/S0927-5193(06)80015-X.

[2] N. Du, H.B. Park, M.M. Dal-Cin, M.D. Guiver, Advances in high permeability polymeric membrane materials for CO_2 separations, Energy Environ. Sci. 5 (2012) 7306–7322, https://doi.org/10.1039/C1EE02668B.

[3] H.B. Park, J. Kamcev, L.M. Robeson, M. Elimelech, B.D. Freeman, Maximizing the right stuff: the trade-off between membrane permeability and selectivity, Science 356 (2017) 1138–1148, https://doi.org/10.1126/science.aab0530.

[4] I. Hossain, K.I. Kim, A. Husna, J.H. Kang, T.-H. Kim, H.B. Park, Metal-coordinated, dual-crosslinked PIM polymer membranes for upgraded CO_2 separation: aging and plasticization resistance, Small 21 (2025) 2407973, https://doi.org/10.1002/smll.202407973.

[5] L.M. Robeson, The upper bound revisited, J. Membr. Sci. 320 (2008) 390–400, https://doi.org/10.1016/j.memsci.2008.04.030.

[6] L.C.E. Struik, Physical Aging in Amorphous Polymers and Other Materials, Elsevier, Amsterdam, 1978.

[7] M.Z. Ahmad, R. Castro-Muñoz, P.M. Budd, Boosting gas separation performance and suppressing the physical aging of polymers of intrinsic microporosity (PIM-1)

by nanomaterial blending, Nanoscale 12 (2020) 23333–23370, https://doi.org/10.1039/D0NR07042D.

[8] R. Swaidan, B. Ghanem, E. Litwiller, I. Pinnau, Physical aging, plasticization and their effects on gas permeation in "rigid" polymers of intrinsic microporosity, Macromolecules 48 (2015) 6553–6561, https://doi.org/10.1021/acs.macromol.5b01581.

[9] S. Guo, J.Y. Yeo, F.M. Benedetti, D. Syar, T.M. Swager, Z.P. Smith, A microporous poly(arylene ether) platform for membrane-based gas separation, Angew. Chem. Int. Ed. 63 (2024), https://doi.org/10.1002/ange.202315611.

[10] D. Zhang, M. Kanezashi, T. Tsuru, K. Yamamoto, T. Gunji, Y. Adachi, J. Ohshita, Preparation of thermally stable 3-glycidyloxypropyl-POSS-derived polysilsesquioxane RO membranes for water desalination, J. Membr. Sci. 668 (2023) 121213, https://doi.org/10.1016/j.memsci.2022.121213.

[11] J. Kim, Y. Park, M.S. Kwon, Recent progress in ladder-like polysilsesquioxane: synthesis and applications, Mater. Chem. Front. (2024), https://doi.org/10.1039/D4QM00197D.

[12] M.G. Mohamed, S.-W. Kuo, Functional polyimide/polyhedral oligomeric silsesquioxane nanocomposites, Polymers 11 (2019) 26, https://doi.org/10.3390/polym11010026.

[13] S.-W. Kuo, F.-C. Chang, POSS related polymer nanocomposites, Prog. Polym. Sci. 36 (2011) 1649–1696, https://doi.org/10.1016/j.progpolymsci.2011.05.002.

[14] S.-W. Kuo, Hydrogen bonding interactions in polymer/polyhedral oligomeric silsesquioxane nanomaterials, J. Polym. Res. 29 (2022) 69, https://doi.org/10.1007/s10965-021-02885-4.

[15] J. Wang, W. Du, Z. Zhang, W. Gao, Z. Li, Biomass/polyhedral oligomeric silsesquioxane nanocomposites: advances in preparation strategies and performances, J. Appl. Polym. Sci. 138 (2021) 49641, https://doi.org/10.1002/app.49641.

[16] M.G. Mohamed, S.-W. Kuo, Functional silica and carbon nanocomposites based on polybenzoxazines, Macromol. Chem. Phys. 220 (2019) 1800306, https://doi.org/10.1002/macp.201800306.

[17] H. Wei, Y. Liu, M. Yuan, G. Shao, Y. Lan, W. Zhang, Viologen based star copolymer membranes: preparation and application in CO_2/CH_4 separation, J. Membr. Sci. 722 (2025) 123872, https://doi.org/10.1016/j.memsci.2025.123872.

[18] M.G. Mohamed, S.-W. Kuo, Polybenzoxazine/polyhedral oligomeric silsesquioxane (POSS) nanocomposites, Polymers 8 (2016) 225, https://doi.org/10.3390/polym8060225.

[19] D. Zhang, M. Kanezashi, T. Tsuru, K. Yamamoto, T. Gunji, Y. Adachi, J. Ohshita, Development of PSQ-RO membranes with high water permeability by copolymerization of bis[3-(triethoxysilyl)propyl]amine and triethoxy(3-glycidyloxypropyl)silane, J. Membr. Sci. 644 (2022) 120162, https://doi.org/10.1016/j.memsci.2021.120162.

[20] S. Neyertz, N.E. Benes, D. Brown, Molecular simulations of hybrid cross-linked membranes for H_2S gas separation at very high temperatures and pressure: binary 90%/10% N_2/H_2S and CH_4/H_2S, ternary 90%/9%/1% $N_2/CO_2/H_2S$ and $CH_4/CO_2/H_2S$ mixtures, J. Membr. Sci. 687 (2023) 122092, https://doi.org/10.1016/j.memsci.2023.122092.

[21] X. Xu, B. Peng, Y. Wang, Y. Dong, H. Wang, W. Chen, Y. Liu, Q. Zhang, Fabrication of POSS-centered polyester network as high anti-chlorine and anti-fouling separation layer of membrane via successive Photo-ATRP and interfacial polymerization for molecular separation, J. Membr. Sci. 715 (2025) 123432, https://doi.org/10.1016/j.memsci.2024.123432.

[22] M.G. Mohamed, S.-W. Kuo, Progress in the self-assembly of organic/inorganic polyhedral oligomeric silsesquioxane (POSS) hybrids, Soft Matter 18 (2022) 5535–5561, https://doi.org/10.1039/D2SM00635A.

[23] C.J. Brinker, GeorgeW. Scherer, Sol-Gel Science: the Physics and Chemistry of Sol-Gel Processing, Elsevier Inc., 2013.

[24] D. Setiawan, W.-H. Chiang, Amine-functionalized biogenic silica derived from rice husk for Pebax-based mixed matrix membranes in CO_2/N_2 separation, J. Membr. Sci. 680 (2023) 121732, https://doi.org/10.1016/j.memsci.2023.121732.

[25] V. Bui, A.M. Tandel, V.R. Satti, E. Haddad, H. Lin, Engineering silica membranes for separation performance, hydrothermal stability, and production scalability, Adv. Membrane 3 (2023) 100064, https://doi.org/10.1016/j.advmem.2023.100064.

[26] G.D. West, G.G. Diamond, D. Holland, M.E. Smith, M.H. Lewis, Gas transport mechanisms through sol–gel derived templated membranes, J. Membr. Sci. 203 (2002) 53–69, https://doi.org/10.1016/S0376-7388(01)00746-3.

[27] H. Nagasawa, R. Yasunari, M. Kawasaki, M. Kanezashi, T. Tsuru, Facile low-temperature route toward the development of polymer-supported silica-based membranes for gas separation via atmospheric-pressure plasma-enhanced chemical vapor deposition, J. Membr. Sci. 638 (2021) 119709, https://doi.org/10.1016/j.memsci.2021.119709.

[28] H. Nagasawa, M. Kawasaki, N. Moriyama, M. Kanezashi, T. Tsuru, Silica-polysiloxane nanocomposite membrane via 2-step atmospheric-pressure PECVD for precise molecular-sieving H_2 separation, Sep. Purif. Technol. 361 (2025) 131631, https://doi.org/10.1016/j.seppur.2025.131631.

[29] B. Ballinger, J. Motuzas, S. Smart, J.C. Diniz da Costa, Palladium cobalt binary doping of molecular sieving silica membranes, J. Membr. Sci. 451 (2014) 185–191, https://doi.org/10.1016/j.memsci.2013.09.057.

[30] J. Wang, Z. Wu, L. Qi, S. Wang, N. Wu, M. Guo, X. Ren, J. Zhong, Bimetallic LaNi-doped silica membranes for hydrogen separation, Fuel 400 (2025) 135762, https://doi.org/10.1016/j.fuel.2025.135762.

[31] I. Rana, H. Nagasawa, T. Tsuru, M. Kanezashi, Tailoring the structure of a sub-nano silica network via fluorine doping to enhance CO_2 separation and evaluating

[32] CO_2 separation performance under dry or wet conditions, J. Membr. Sci. 658 (2022) 120735, https://doi.org/10.1016/j.memsci.2022.120735.

[32] P. Muthukumar, M. Linder, R. Mertz, E. Laurien, Measurement of thermodynamic properties of some hydrogen absorbing alloys, Int. J. Hydrogen Energy 34 (2009) 1873–1879, https://doi.org/10.1016/j.ijhydene.2008.12.052.

[33] X. Yang, Q. Hou, L. Yu, J. Zhang, Improvement of the hydrogen storage characteristics of MgH_2 with a flake Ni nano-catalyst composite, Dalton Trans. 50 (2021) 1797.

[34] V. Boffa, D.H.A. Blank, J.E. ten Elshof, Hydrothermal stability of microporous silica and niobia–silica membranes, J. Membr. Sci. 319 (2008) 256–263, https://doi.org/10.1016/j.memsci.2008.03.042.

[35] M. Kanezashi, M. Asaeda, Hydrogen permeation characteristics and stability of Ni-doped silica membranes in steam at high temperature, J. Membr. Sci. 271 (2006) 86–93, https://doi.org/10.1016/j.memsci.2005.07.011.

[36] N. Kageyama, A. Takagaki, T. Sugawara, R. Kikuchi, S.T. Oyama, Synthesis and characterization of a silica-alumina composite membrane and its application in a membrane reactor, Sep. Purif. Technol. 195 (2018) 437–445, https://doi.org/10.1016/j.seppur.2017.12.021.

[37] F. Jiang, J. Yang, M. Yan, Enhancement strategy for superior H_2/CO_2 separation with binary Ag-MgO doped silica membranes, J. Membr. Sci. 734 (2025) 124392, https://doi.org/10.1016/j.memsci.2025.124392.

[38] D. Gnanasekaran, A. Shanavas, W.W. Focke, R. Sadiku, Polyhedral oligomeric silsesquioxane/polyamide bio-nanocomposite membranes: structure-gas transport properties, RSC Adv. 5 (2015) 11272–11283, https://doi.org/10.1039/C4RA12716A.

[39] N.B. McKeown, P.M. Budd, Polymers of intrinsic microporosity (PIMs): organic materials for membrane separations, heterogeneous catalysis and hydrogen storage, Chem. Soc. Rev. 35 (2006) 675–683, https://doi.org/10.1039/B600349D.

[40] N.B. McKeown, P.M. Budd, Exploitation of intrinsic microporosity in polymer-based materials, Macromolecules 43 (2010) 5163–5176, https://doi.org/10.1021/ma1006396.

[41] W.F. Yong, K.H.A. Kwek, K.-S. Liao, T.-S. Chung, Suppression of aging and plasticization in highly permeable polymers, Polymer 77 (2015) 377–386, https://doi.org/10.1016/j.polymer.2015.09.075.

[42] N. Konnertz, Y. Ding, W.J. Harrison, P.M. Budd, A. Schönhals, M. Böhning, Molecular mobility and gas transport properties of nanocomposites based on PIM-1 and polyhedral oligomeric phenethyl-silsesquioxanes (POSS), J. Membr. Sci. 529 (2017) 274–285, https://doi.org/10.1016/j.memsci.2017.02.007.

[43] Y. Kinoshita, K. Wakimoto, A.H. Gibbons, A.P. Isfahani, H. Kusuda, E. Sivaniah, B. Ghalei, Enhanced PIM-1 membrane gas separation selectivity through efficient dispersion of functionalized POSS fillers, J. Membr. Sci. 539 (2017) 178–186, https://doi.org/10.1016/j.memsci.2017.05.072.

[44] S. Mohsenpour, A.W. Ameen, S. Leaper, C. Skuse, F. Almansour, P.M. Budd, P. Gorgojo, PIM-1 membranes containing POSS-graphene oxide for CO_2 separation, Sep. Purif. Technol. 298 (2022) 121447, https://doi.org/10.1016/j.seppur.2022.121447.

[45] H. Lin, B.D. Freeman, Gas solubility, diffusivity and permeability in poly(ethylene oxide), J. Membr. Sci. 239 (2004) 105–117, https://doi.org/10.1016/j.memsci.2003.08.031.

[46] D. Polak, M. Szwast, Material and process tests of heterogeneous membranes containing ZIF-8, SiO_2 and POSS-Ph, Materials 15 (2022) 6455, https://doi.org/10.3390/ma15186455.

[47] MdM. Rahman, V. Filiz, S. Shishatskiy, C. Abetz, S. Neumann, S. Bolmer, M. M. Khan, V. Abetz, PEBAX® with PEG functionalized POSS as nanocomposite membranes for CO_2 separation, J. Membr. Sci. 437 (2013) 286–297, https://doi.org/10.1016/j.memsci.2013.03.001.

[48] J.H. Shin, H.J. Yu, H. An, A.S. Lee, S.S. Hwang, S.Y. Lee, J.S. Lee, Rigid double-stranded siloxane-induced high-flux carbon molecular sieve hollow fiber membranes for CO_2/CH_4 separation, J. Membr. Sci. 570–571 (2019) 504–512, https://doi.org/10.1016/j.memsci.2018.10.076.

[49] J.H. Shin, H.J. Yu, J Park, A.S. Lee, S.S. Hwang, S.-J. Kim, S. Park, K.Y. Cho, W. Won, J.S. Lee, Fluorine-containing polyimide/polysilsesquioxane carbon molecular sieve membranes and techno-economic evaluation thereof for C_3H_6/C_3H_8 separation, J. Membr. Sci. 598 (2020) 117660, https://doi.org/10.1016/j.memsci.2019.117660.

[50] W.J. Koros, C. Zhang, Materials for next-generation molecularly selective synthetic membranes, Nat. Mater. 16 (2017) 289–297, https://doi.org/10.1038/nmat4805.

[51] L. Xu, M. Rungta, W.J. Koros, Matrimid® derived carbon molecular sieve hollow fiber membranes for ethylene/ethane separation, J. Membr. Sci. 380 (2011) 138–147, https://doi.org/10.1016/j.memsci.2011.06.037.

[52] C.-C. Chen, W. Qiu, S.J. Miller, W.J. Koros, Plasticization-resistant hollow fiber membranes for CO_2/CH_4 separation based on a thermally crosslinkable polyimide, J. Membr. Sci. 382 (2011) 212–221, https://doi.org/10.1016/j.memsci.2011.08.015.

[53] T.S. Haddad, J.D. Lichtenhan, Hybrid organic−inorganic thermoplastics: Styryl-based polyhedral oligomeric silsesquioxane polymers, Macromolecules 29 (1996) 7302–7304, https://doi.org/10.1021/ma960609d.

[54] G. Li, L. Wang, H. Ni, C.U. Pittman, Polyhedral oligomeric silsesquioxane (POSS) polymers and copolymers: a review, J. Inorg. Organomet. Polym. Mater. 11 (2001) 123–154, https://doi.org/10.1023/A:1015287910502.

[55] A. Romo-Uribe, P.T. Mather, T.S. Haddad, J.D. Lichtenhan, Viscoelastic and morphological behavior of hybrid styryl-based polyhedral oligomeric silsesquioxane (POSS) copolymers, J. Polym. Sci. 36 (1998) 1857–1872, https://doi.org/10.1002/polb.1998.36.issue-11.

[56] H. Xu, S.-W. Kuo, F.-C. Chang, Poly(acetoxystyrene-co-isobutylstyryl POSS) nanocomposites: characterization and molecular interaction, J. Polym. Res. 9 (2002) 239–244, https://doi.org/10.1023/A:1021303818406.

[57] Y. Zhu, J. Zhao, X. Wang, Q. Li, Synthesis and luminescent property of polycarbazole/polyhedral oligomeric silsesquioxane nanocomposites, Chem. Res. Chin. Univ. 24 (2008) 570–574, https://doi.org/10.1016/S1005-9040(08)60120-8.

[58] Y.-J. Lee, J.-M. Huang, S.-W. Kuo, F.-C. Chang, Low-dielectric, nanoporous polyimide films prepared from PEO–POSS nanoparticles, Polymer 46 (2005) 10056–10065, https://doi.org/10.1016/j.polymer.2005.08.047.

[59] R. Verker, E. Grossman, N. Eliaz, Erosion of POSS-polyimide films under hypervelocity impact and atomic oxygen: the role of mechanical properties at elevated temperatures, Acta Mater. 57 (2009) 1112–1119, https://doi.org/10.1016/j.actamat.2008.10.054.

[60] S. Wu, T. Hayakawa, M. Kakimoto, H. Oikawa, Synthesis and characterization of organosoluble aromatic polyimides containing POSS in main chain derived from double-decker-shaped silsesquioxane, Macromolecules 41 (2008) 3481–3487, https://doi.org/10.1021/ma7027227.

[61] J. Huang, P.C. Lim, L. Shen, P.K. Pallathadka, K. Zeng, C. He, Cubic silsesquioxane–polyimide nanocomposites with improved thermomechanical and dielectric properties, Acta Mater. 53 (2005) 2395–2404, https://doi.org/10.1016/j.actamat.2005.02.001.

[62] B. Dasgupta, S.K. Sen, S. Banerjee, Aminoethylaminopropylisobutyl POSS–polyimide nanocomposite membranes and their gas transport properties, Mater. Sci. Eng. B 168 (2010) 30–35, https://doi.org/10.1016/j.mseb.2009.10.006.

[63] H. Ríos-Dominguez, F.A. Ruiz-Treviño, R. Contreras-Reyes, A. González-Montiel, Syntheses and evaluation of gas transport properties in polystyrene–POSS membranes, J. Membr. Sci. 271 (2006) 94–100, https://doi.org/10.1016/j.memsci.2005.07.014.

[64] A.F. Ismail, W. Lorna, Penetrant-induced plasticization phenomenon in glassy polymers for gas separation membrane, Sep. Purif. Technol. 27 (2002) 173–194, https://doi.org/10.1016/S1383-5866(01)00211-8.

[65] M.L. Chua, L. Shao, B.T. Low, Y. Xiao, T.-S. Chung, Polyetheramine–polyhedral oligomeric silsesquioxane organic–inorganic hybrid membranes for CO_2/H_2 and CO_2/N_2 separation, J. Membr. Sci. 385–386 (2011) 40–48, https://doi.org/10.1016/j.memsci.2011.09.008.

[66] F. Li, Y. Li, T.-S. Chung, S. Kawi, Facilitated transport by hybrid POSS®–Matrimid®–Zn^{2+} nanocomposite membranes for the separation of natural gas, J. Membr. Sci. 356 (2010) 14–21, https://doi.org/10.1016/j.memsci.2010.03.021.

[67] P. Iyer, G. Iyer, M. Coleman, Gas transport properties of polyimide–POSS nanocomposites, J. Membr. Sci. 358 (2010) 26–32, https://doi.org/10.1016/j.memsci.2010.04.023.

[68] K. Li, X. Lv, J. Wang, L. Li, F. Chen, J. Wang, Z. Wang, X. Li, Low-resistance transport pathways in POSS/CPBI mixed matrix membranes for efficient CO_2 separation, ACS Appl. Nano Mater. 6 (2023) 11822–11829, https://doi.org/10.1021/acsanm.3c01733.

[69] H.J. Yu, C.-H. Chan, S.Y. Nam, S.-J. Kim, J.S. Yoo, J.S. Lee, Thermally cross-linked ultra-robust membranes for plasticization resistance and permeation enhancement – a combined theoretical and experimental study, J. Membr. Sci. 646 (2022) 120250, https://doi.org/10.1016/j.memsci.2021.120250.

[70] Y.Y. Jo, A.S. Lee, K.-Y. Baek, H. Lee, S.S. Hwang, Thermally reversible self-healing polysilsesquioxane structure-property relationships based on Diels-Alder chemistry, Polymer 108 (2017) 58–65, https://doi.org/10.1016/j.polymer.2016.11.040.

[71] Y.H. Kim, G.M. Choi, J.G. Bae, Y.H. Kim, B.S. Bae, High-performance and simply-synthesized ladder-like structured methacrylate siloxane hybrid material for flexible hard coating, Polymers 10 (2018) 449, https://doi.org/10.3390/polym10040449.

[72] K.I. Jung, S.O. Hwang, N.H. Kim, D.G. Lee, J.-H. Lee, H.W. Jung, Effect of methacryloxypropyl and phenyl functional groups on crosslinking and rheological and mechanical properties of ladder-like polysilsesquioxane hard coatings, Prog. Org. Coating 124 (2018) 129–136, https://doi.org/10.1016/j.porgcoat.2018.08.005.

[73] R.M. de Vos, H. Verweij, High-selectivity, high-flux silica membranes for gas separation, Science 279 (1998) 1710–1711, https://doi.org/10.1126/science.279.5357.1710.

[74] S.J. Khatib, S.T. Oyama, Silica membranes for hydrogen separation prepared by chemical vapor deposition (CVD), Sep. Purif. Technol. 111 (2013) 20–42, https://doi.org/10.1016/j.seppur.2013.03.032.

[75] A. Ayral, C. Balzer, T. Dabadie, C. Guizard, A. Julbe, Sol-gel derived silica membranes with tailored microporous structures, Catal. Today 25 (1995) 219–224, https://doi.org/10.1016/0920-5861(95)00081-P.

[76] J.R. Uhlhorn, K. Keizer, A.J. Burggraaf, Gas transport and separation with ceramic membranes. Part II. Synthesis and separation properties of microporous membranes, J. Membr. Sci. 66 (1992) 271–287.

[77] H.J. Frost, R. Raj, Limiting densities for dense random packing of spheres, J. Am. Ceram. Soc. 65 (1982), https://doi.org/10.1111/j.1151-2916.1982.tb10371.x. C-19-C-21.

[78] G. Ji, X. Gao, S. Smart, S.K. Bhatia, G. Wang, K. Hooman, J.C. Diniz da Costa, Estimation of pore size distribution of amorphous silica-based membrane by the activation energies of gas permeation, Processes 6 (2018).

[79] M. Guo, J. Qian, R. Xu, X. Ren, J. Zhong, M. Kanezashi, Boosting the CO_2 capture efficiency through aromatic bridged organosilica membranes, J. Membr. Sci. 643 (2022) 120018.

[80] H.L. Castricum, G.G. Paradis, M.C. Mittelmeijer-Hazeleger, R. Kreiter, J.F. Vente, J.E. Ten Elshof, Tailoring the separation behavior of hybrid organosilica membranes by adjusting the structure of the organic bridging group, Adv. Funct. Mater. 21 (2011) 2319–2329, https://doi.org/10.1002/adfm.201002361.

[81] H.L. Castricum, A. Sah, R. Kreiter, D.H.A. Blank, J.F. Vente, J.E. ten Elshof, Hybrid ceramic nanosieves: stabilizing nanopores with organic links, Chem. Commun. (2008) 1103–1105, https://doi.org/10.1039/B718082A.

[82] M. Kanezashi, Y. Yoneda, H. Nagasawa, T. Tsuru, K. Yamamoto, J. Ohshita, Gas permeation properties for organosilica membranes with different Si/C ratios and evaluation of microporous structures, AIChE J. 63 (2017) 4491–4498, https://doi.org/10.1002/aic.15778.

[83] L. Yu, M. Kanezashi, H. Nagasawa, T. Tsuru, Fabrication and CO_2 permeation properties of amine-silica membranes using a variety of amine types, J. Membr. Sci. 541 (2017) 447–456, https://doi.org/10.1016/j.memsci.2017.07.024.

[84] S.B. Messaoud, A. Takagaki, T. Sugawara, R. Kikuchi, S.T. Oyama, Alkylamine–silica hybrid membranes for carbon dioxide/methane separation, J. Membr. Sci. 477 (2015) 161–171, https://doi.org/10.1016/j.memsci.2014.12.022.

[85] K. Yoshida, Y.H. Ikuhara, S. Takahashi, T. Hirayama, T. Saito, S. Sueda, N. Tanaka, P.L. Gai, The three-dimensional morphology of nickel nanodots in amorphous silica and their role in high-temperature permselectivity for hydrogen separation, Nanotechnology 20 (2009) 315703, https://doi.org/10.1088/0957-4484/20/31/31570.

[86] C. Yacou, S. Smart, J.C. Diniz da Costa, Long term performance cobalt oxide silica membrane module for high temperature H_2 separation, Energy Environ. Sci. 5 (2012) 5820–5832, https://doi.org/10.1039/C2EE03247C.

[87] M.W.J. Luiten, N.E. Benes, C. Huiskes, H. Kruidhof, A. Nijmeijer, Robust method for micro-porous silica membrane fabrication, J. Membr. Sci. 348 (2010) 1–5, https://doi.org/10.1016/j.memsci.2009.11.029.

[88] M. Nomura, T. Nagayo, K. Monma, Pore size control of a molecular sieve silica membrane prepared by a counter diffusion CVD method, J. Chem. Eng. Jpn. 40 (2007) 1235–1241, https://doi.org/10.1252/jcej.07WE065.

[89] M. Nomura, Preparation of silica membranes by CVD method, in: Silica Membranes: Preparation, Modelling, Application, and Commercialization (Current Trends and Future Developments on (Bio-) Membranes), Elsevier, 2017, pp. 25–43, https://doi.org/10.1016/B978-0-444-63866-3.00002-9.

[90] N. Bighane, W.J. Koros, Novel silica membranes for high temperature gas separations, J. Membr. Sci. 371 (2011) 254–262, https://doi.org/10.1016/j.memsci.2011.01.045.

[91] J. Adams, N. Bighane, W.J. Koros, Pore morphology and temperature dependence of gas transport properties of silica membranes derived from oxidative thermolysis of polydimethylsiloxane, J. Membr. Sci. 524 (2017) 585–595, https://doi.org/10.1016/j.memsci.2016.11.074.

[92] M. Kanezashi, T. Sasaki, H. Tawarayama, H. Nagasawa, T. Yoshioka, K. Ito, T. Tsuru, Experimental and theoretical study on small gas permeation properties through amorphous silica membranes fabricated at different temperatures, J. Phys. Chem. C 118 (2014) 20323–20331, https://doi.org/10.1021/jp504937t.

[93] T. Yoshioka, E. Nakanishi, T. Tsuru, M. Asaeda, Experimental studies of gas permeation through microporous silica membranes, AIChE J. 47 (2001) 2052–2063, https://doi.org/10.1002/aic.690470916.

[94] T. Yoshioka, M. Asaeda, T. Tsuru, A molecular dynamics simulation of pressure-driven gas permeation in a micropore potential field on silica membranes, J. Membr. Sci. 293 (2007) 81–93, https://doi.org/10.1016/j.memsci.2007.01.039.

[95] M.H. Hassan, J. Douglas Way, P.M. Thoen, A.C. Dillon, Single component and mixed gas transport in a silica hollow fiber membrane, J. Membr. Sci. 104 (1995) 27–42, https://doi.org/10.1016/0376-7388(95)00009-2.

[96] M. Kanezashi, T. Matsutani, T. Wakihara, H. Nagasawa, T. Okubo, T. Tsuru, Preparation and gas permeation properties of fluorine–silica membranes with controlled amorphous silica structures: effect of fluorine source and calcination temperature on network size, ACS Appl. Mater. Interfaces 9 (2017) 24625–24633, https://doi.org/10.1021/acsami.7b06800.

[97] M. Kanezashi, T. Sasaki, H. Tawarayama, T. Yoshioka, T. Tsuru, Hydrogen permeation properties and hydrothermal stability of Sol–gel-derived amorphous silica membranes fabricated at high temperatures, J. Am. Ceram. Soc. 96 (2013) 2950–2957, https://doi.org/10.1111/jace.12523.

[98] H. Qi, J. Han, N. Xu, Effect of calcination temperature on carbon dioxide separation properties of a novel microporous hybrid silica membrane, J. Membr. Sci. 382 (2011) 231–237, https://doi.org/10.1016/j.memsci.2011.08.013.

[99] H. Yong Ha, S. Woo Nam, S.-A. hong, W. Kook Lee, Chemical vapor deposition of hydrogen-permselective silica films on porous glass supports from tetraethylorthosilicate, J. Membr. Sci. 85 (1993) 279–290, https://doi.org/10.1016/0376-7388(93)85281-Z.

[100] K. Akamatsu, M. Suzuki, A. Nakao, S. Nakao, Development of hydrogen-selective dimethoxydimethylsilane-derived silica membranes with thin active separation layer by chemical vapor deposition, J. Membr. Sci. 580 (2019) 268–274, https://doi.org/10.1016/j.memsci.2019.03.024.

[101] H. Kato, S.-T.B. Lundin, S.-J. Ahn, A. Takagaki, R. Kikuchi, S.T. Oyama, Gas separation silica membranes prepared by chemical vapor deposition of methyl-substituted silanes, Membranes 9 (2019), https://doi.org/10.3390/membranes9110144.

[102] G. Li, M. Kanezashi, T. Tsuru, Preparation of organic–inorganic hybrid silica membranes using organoalkoxysilanes: the effect of pendant groups, J. Membr. Sci. 379 (2011) 287–295, https://doi.org/10.1016/j.memsci.2011.05.071.

[103] C.R. Miller, D.K. Wang, S. Smart, J.C. Diniz da Costa, Reversible redox effect on gas permeation of cobalt doped ethoxy polysiloxane (ES40) membranes, Sci. Rep. 3 (2013) 1648, https://doi.org/10.1038/srep01648.

[104] U. Anggarini, H. Nagasawa, M. Kanezashi, T. Tsuru, Structural two-phase evolution of aminosilica-based silver-coordinated membranes for increased hydrogen separation, J. Membr. Sci. 642 (2022) 119962, https://doi.org/10.1016/j.memsci.2021.119962.

[105] N. Rafia, A.A. Babaluo, K. Ghasemzadeh, Enhanced hydrogen separation performance of cobalt-doped microporous silica membranes: influence of cobalt content and processing parameters, Int. J. Hydrogen Energy 95 (2024) 1194–1203, https://doi.org/10.1016/j.ijhydene.2024.07.048.

[106] X. Yu, L. Meng, T. Niimi, H. Nagasawa, M. Kanezashi, T. Yoshioka, T. Tsuru, Network engineering of a BTES-E membrane for improved gas performance via a novel pH-swing method, J. Membr. Sci. 511 (2016) 219–227, https://doi.org/10.1016/j.memsci.2016.03.060.

[107] H.F. Qureshi, R. Besselink, J.E. ten Elshof, A. Nijmeijer, L. Winnubst, Doped microporous hybrid silica membranes for gas separation, J. Sol. Gel Sci. Technol. 75 (2015) 180–188, https://doi.org/10.1007/s10971-015-3647-3.

[108] H. Song, S. Zhao, J. Lei, C. Wang, H. Qi, Pd-doped organosilica membrane with enhanced gas permeability and hydrothermal stability for gas separation, J. Mater. Sci. 51 (2016) 6275–6286, https://doi.org/10.1007/s10853-016-9863-y.

[109] D. Lee, L. Zhang, S.T. Oyama, S. Niu, R.F. Saraf, Synthesis, characterization, and gas permeation properties of a hydrogen-permeable silica membrane supported on porous alumina, J. Membr. Sci. 231 (2004) 117–126, https://doi.org/10.1016/j.memsci.2003.10.044.

[110] G. Polotskaya, M. Goikhman, I. Podeshvo, V. Kudryavtsev, Z. Pientka, L. Brozova, M. Bleha, Gas transport properties of polybenzoxazinoneimides and their prepolymers, Polymer 46 (2005) 3730–3736, https://doi.org/10.1016/j.polymer.2005.02.111.

[111] M.E. Rezac, B. Schöberl, Transport and thermal properties of poly(ether imide)/acetylene-terminated monomer blends, J. Membr. Sci. 156 (1999) 211–222, https://doi.org/10.1016/S0376-7388(98)00346-9.

[112] D. Fritsch, N. Avella, Synthesis and properties of highly gas permeable poly (amide-imide)s, Macromol. Chem. Phys. 197 (1996) 2217–2227, https://doi.org/10.1002/macp.1996.021970224.

[113] P.M. Budd, K.J. Msayib, C.E. Tattershall, B.S. Ghanem, K.J. Reynolds, N. B. McKeown, D. Fritsch, Gas separation membranes from polymers of intrinsic microporosity, J. Membr. Sci. 251 (2005) 263–269, https://doi.org/10.1016/j.memsci.2005.01.009.

[114] K. Nagai, A. Higuchi, T. Nakagawa, Gas permeability and stability of poly(1-trimethylsilyl-1-propyne-co-1-phenyl-1-propyne) membranes, J. Polym. Sci. B Polym. Phys. 33 (1995) 289–298, https://doi.org/10.1002/polb.1995.090330214.

[115] C.M. Zimmerman, W.J. Koros, Polypyrrolones for membrane gas separations. I. Structural comparison of gas transport and sorption properties, J. Polym. Sci. B Polym. Phys. 37 (37:12) (1999) 1235–1249, https://doi.org/10.1002/(SICI)1099-0488(19990615).

[116] L. Yang, J. Fang, N. Meichin, K. Tanaka, H. Kita, K. Okamoto, Gas permeation properties of thianthrene-5,5,10,10-tetraoxide-containing polyimides, Polymer 42 (2001) 2021–2029, https://doi.org/10.1016/S0032-3861(00)00500-0.

[117] Y. Shida, T. Sakaguchi, M. Shiotsuki, F. Sanda, B.D. Freeman, T. Masuda, Synthesis and properties of membranes of poly(diphenylacetylenes) having fluorines and hydroxyl groups, Macromolecules 39 (2006) 569–574, https://doi.org/10.1021/ma052082n.

[118] L. Wang, Y. Cao, M. Zhou, S.J. Zhou, Q. Yuan, Novel copolyimide membranes for gas separation, J. Membr. Sci. 305 (2007) 338–346, https://doi.org/10.1016/j.memsci.2007.08.024.

[119] M. Al-Masri, H.R. Kricheldorf, D. Fritsch, New polyimides for gas separation. 1. Polyimides derived from substituted terphenylenes and 4,4'-(hexafluoroisopropylidene)diphtalic anhydride, Macromolecules 32 (1999) 7853–7858, https://doi.org/10.1021/ma9910742.

[120] C. Nagel, K. Günther-Schade, D. Fritsch, T. Strunskus, F. Faupel, Free volume and transport properties in highly selective polymer membranes, Macromolecules 35 (2002) 2071–2077, https://doi.org/10.1021/ma011028d.

[121] T. Mizumoto, T. Masuda, T. Higashimura, Polymerization of [o-(trimethylgermyl) phenyl] acetylene and polymer characterization, J. Polym. Sci. Polym. Chem. 31 (1993) 2555–2561, https://doi.org/10.1002/pola.1993.080311016.

[122] J. Yu, H.-K. Lim, S. Lee, Transition-metal softener for high-durability hydrogen separation silica membranes, J. Phys. Chem. C 123 (2019) 25761–25768, https://doi.org/10.1021/acs.jpcc.9b08068.

[123] M. Tsapatsis, G. Gavalas, Structure and aging characteristics of H$_2$-permselective SiO$_2$-Vycor membranes, J. Membr. Sci. 87 (1994) 281–296, https://doi.org/10.1016/0376-7388(94)87034-9.

[124] G.P. Fotou, Y.S. Lin, S.E. Pratsinis, Hydrothermal stability of pure and modified microporous silica membranes, J. Mater. Sci. 30 (1995) 2803–2808, https://doi.org/10.1007/BF00349647.

[125] R.M. de Vos, W.F. Maier, H. Verweij, Hydrophobic silica membranes for gas separation, J. Membr. Sci. 158 (1999) 277–288, https://doi.org/10.1016/S0376-7388(99)00035-6.

[126] Q. Wei, F. Wang, Z.-R. Nie, C.-L. Song, Y.-L. Wang, Q.-Y. Li, Highly hydrothermally stable microporous silica membranes for hydrogen separation, J. Phys. Chem. B 112 (2008) 9354–9359, https://doi.org/10.1021/jp711573f.

[127] M. ten Hove, M.W.J. Luiten-Olieman, C. Huiskes, A. Nijmeijer, L. Winnubst, Hydrothermal stability of silica, hybrid silica and Zr-doped hybrid silica membranes, Sep. Purif. Technol. 189 (2017) 48–53, https://doi.org/10.1016/j.seppur.2017.07.045.

[128] J.E. ten Elshof, A.P. Dral, Structure–property tuning in hydrothermally stable sol–gel-processed hybrid organosilica molecular sieving membranes, J. Sol. Gel Sci. Technol. 79 (2016) 279–294.

[129] C. Barboiu, B. Sala, S. Bec, S. Pavan, E. Petit, Ph Colomban, J. Sanchez, S. de Perthuis, D. Hittner, Structural and mechanical characterizations of microporous silica–boron membranes for gas separation, J. Membr. Sci. 326 (2009).

[130] H.L. Castricum, A. Sah, R. Kreiter, D.H.A. Blank, J.F. Vente, J.E. ten Elshof, Hydrothermally stable molecular separation membranes from organically linked silica, J. Mater. Chem. 18 (2008) 2150–2158, https://doi.org/10.1039/B801972J.

[131] D.A. Loy, K.J. Shea, Bridged Polysilsesquioxanes, Highly porous hybrid organic-inorganic materials, Chem. Rev. 95 (1995) 1431–1442, https://doi.org/10.1021/cr00037a013.

[132] K.J. Shea, D.A. Loy, Bridged Polysilsesquioxanes, Molecular-engineered hybrid organic–inorganic materials, Chem. Mater. 13 (2001) 3306–3319, https://doi.org/10.1021/cm011074s.

[133] X. Ren, M. Kanezashi, H. Nagasawa, R. Xu, J. Zhong, T. Tsuru, Ceramic-supported polyhedral oligomeric silsesquioxane-organosilica nanocomposite membrane for efficient gas separation, Ind. Eng. Chem. Res. 58 (2019) 21708–21716.

[134] M. Kanezashi, T. Shioda, T. Gunji, T. Tsuru, Gas permeation properties of silica membranes with uniform pore sizes derived from polyhedral oligomeric silsesquioxane, AIChE J. 58 (2012) 1733–1743.